DYNAMIC RESPONSE ANALYSIS OF SATURATED GRANULAR SOILS TO BLAST LOADS USING A SINGLE PHASE MODEL

A Research Report Submitted to NSERC

by

Guoxi Wu, Ph.D.

NSERC Industrial Research Fellow

Reviewed by:

W. Blair Gohl, Ph.D., P.Eng.

W. Scott Dunbar, Ph.D., P.Eng.

AGRA Earth & Environmental Limited
2227 Douglas Road, Burnaby, BC, V5C 5A9
(604) 294-3811

December 20, 1995

Guoxi
Dec. 29, 1995.

ABSTRACT:

After completing several medium to large sand compaction projects in North America using the blast densification technique, AGRA Earth and Environmental Ltd has launched a research program to study the soil dynamics involved in the blasting process and to provide theoretical support for the use of the method in practice. This research program is financially supported by the Natural Sciences and Engineering Research Council of Canada (NSERC) by means of an Industrial Research Fellowship.

This report presents a numerical model developed through the research program for the analysis of non-linear granular soil response to blast loads. The model uses a three dimensional spherically symmetric finite element formulation. The saturated soil medium is treated as a bonded single phase material. A non-linear shear stress-strain relationship is used to simulate the shear resistance of the material to shear strain, and viscosity is used to model the dependence of the shear resistance of the granular material to the time rate of shear strain.

The finite element formulation has been checked against the closed-form solution by Sharpe (1942) for a linear elastic medium. The finite element method is then used to analyze the nonlinear response of saturated soil media subjected to blast loads. Typical results obtained from this analysis are peak dynamic water pressures, particle velocities, accelerations, volumetric strains, and shear strains versus the scaled distance $R/W^{0.333}$ (where R is the hypocentral distance between the blast and observation point and W is the charge weight). Tentative relationships between peak soil response and scaled distance are presented for water, saturated loose sand and saturated dense sand.

Current research is underway to predict the residual pore water pressure and the permanent ground settlement induced by blast loads. Methods of superimposing the effects of multiple charge detonations are also being examined. The final results of the ongoing research will be presented in the next report to NSERC.

TABLE OF CONTENTS

1.0 INTRODUCTION

Saturated loose sands are susceptible to liquefaction under static or cyclic loading. Liquefaction of sands results in significant loss of shear strength and may lead to failure of earth structures. Various densification techniques have been used to improve the liquefaction resistance of sands by compacting the sands to a more dense state. The use of controlled blasting or explosive compaction is one of these techniques. The major advantages for using the method are that it is cost-effective and can be carried out to significant depths relative to more conventional ground densification techniques such as vibro-flotation, vibro-replacement and dynamic compaction. In addition to reducing the liquefaction potential of loose granular soils, densification can also increase the bearing capacity and limit settlement due to static loading. However, the use of explosive compaction requires expertise with the design of the layout and detonation sequence of the explosives and one must pay careful attention to off-site vibration control and the effects of blasting on slopes or other structures. Development of a numerical model to predict the dynamic soil response is therefore considered will facilitate the blast design process.

Blast densification uses the energy released by detonations of explosives buried within saturated granular soils to shock the soil particles into a denser state of packing. Blast densification has been successfully used over the past 50 years throughout the world. The first successful use of blast densification occurred in the late 1930's where the method was used to densify the foundation soils for the Franklin Falls Dam, New Hampshire (Lyman, 1942). A settlement of up to 10% of the thickness of the sand layer treated was achieved. Following the work at the Franklin Falls Dam, other successful case histories have included:

- foundation densification for the Karnafuli Dam (Hall, 1962)
- foundation densification for electrical transmission towers in Massachusetts (Wild and Haslam, 1962)
- densification of offshore soils at the Port of Amsterdam (Barendsen and Kok, 1983)
- tailings sand densification (Klohn et al., 1981)
- foundation densification for the Jebba dam (Solymar et al., 1984)
- densification of the internal sand core of the Molikpaq off-shore platform (Rogers et al., 1988).
- densification of foundations for bridge end fills, Mt. St. Helens, Washington (Hachey et al, 1993)
- densification of warehouse foundations in an urban setting, New Westminster, B.C. (Gohl et al, 1994)
- densification of cofferdam foundations, SM-3 Dam, Quebec (Ground Engineering, 1995)

In the above projects, settlements in the range of 2% to 8% of the sand layer thickness and post-blast relative densities in the range of 65-85% were achieved for the densified layers.

The detonation of buried explosives (commonly called charges) produces a high-pressure shock wave that propagates radially away from the charges and generates a dynamic pressure pulse within a soil mass. Cole (1948) found that in water, the peak dynamic pressure may exceed 10,500 kPa at 4 m away from a 1 kg charge. The duration of this high pressure pulse is generally under one millisecond (10^{-3} sec), a very short time within which significant drainage of pore water does not usually occur. However, the passage of this high pressure pulse causes large shear and volumetric strain pulses to occur within the soil. Within saturated soils and assuming essentially undrained conditions, the tendency for volumetric contraction of the soil particles generates residual pore water pressures and causes soil liquefaction in the vicinity of the blast.

The present report presents a numerical model for the analysis of granular soil response under blast loads. Using the model, dynamic displacements, velocities and accelerations acting in the radial direction from the charge are computed using a three dimensional, spherically symmetric finite element formulation. The saturated soil medium is treated as a bonded single phase material. A nonlinear shear stress-shear strain relationship is used to describe the shear resistance of the material. A soil-water viscosity term is also used to model the dependence of the shear resistance of the granular material to the time rate of shear strain.

The numerical model has been used to produce tentative relationships between peak dynamic water pressure, particle velocity and acceleration, volumetric strain, and shear strain versus the scaled distance $R/W^{0.333}$ for water, saturated loose sand and saturated dense sand. These relationships have been found useful in blast design and will be progressively refined based on field experience with the blast densification technique.

2.0 DYNAMIC RESPONSE OF A LINEAR ELASTIC MEDIUM SUBJECTED TO BLAST LOADS

2.1 The Idealized Mechanical Model

The idealized model consists of a homogenous elastic infinite medium which has a mass density ρ, a compressive wave velocity V_P, a shear wave velocity V_S and a spherical cavity of radius a. The basic study problem is to find the elastic dynamic response in the medium which results from application of an arbitrary transient pressure p(t) on the interior surface of the cavity. The idealized mechanical model is shown schematically in Figure 2.1.

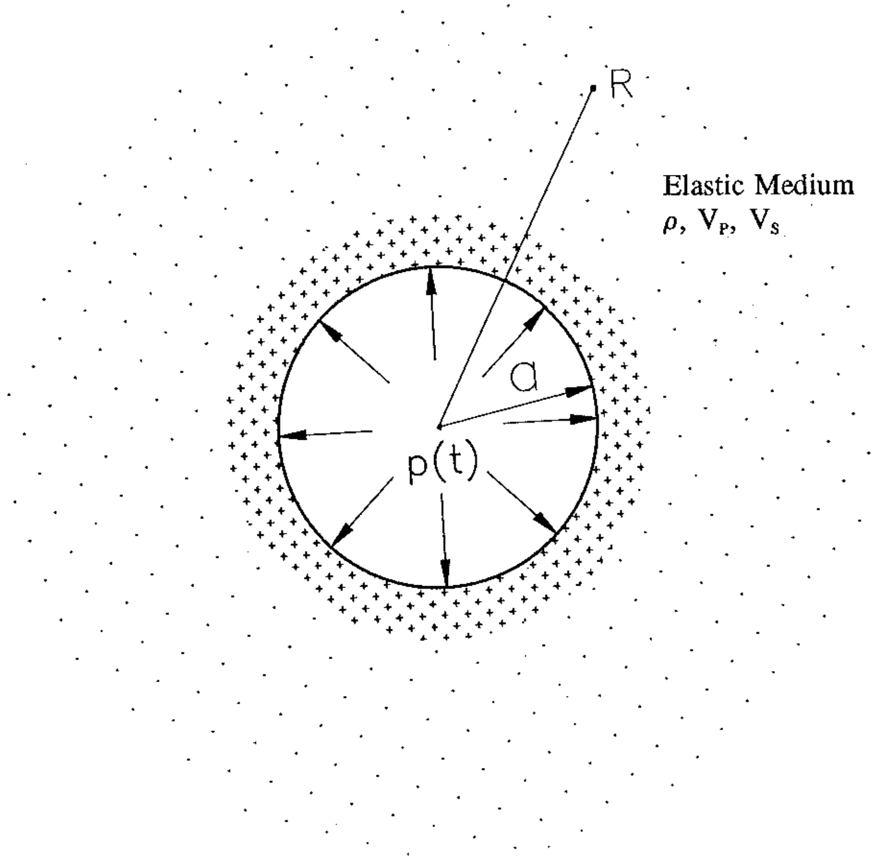

Figure 2.1 The Idealized Mechanical Model

The above elastic model has been extensively described in the engineering literature (Sharpe, 1942) and has been found useful to verify the accuracy of the finite element model developed in the present research program. The important effects of soil nonlinearity and viscosity on dynamic response are taken into account in a later chapter.

Several assumptions have been made to model the dynamic soil response to blast-induced cavity expansion. In this model, the high pressure gas and water filled cavity resulting from detonation of a buried charge has been replaced by an empty, spherical cavity with a uniform pressure acting on the interior surface of the cavity. This idealization ignores the possible effects of different cavity shapes due to blasting, the effect of residual gas and water pressures within the cavity following the blast, and the effects of cavity collapse following blasting due to soil-water flow. Neglect of the latter two effects is not believed significant insofar as modelling far field soil response within a few borehole diameters from a charge. Previous research has suggested that the idealization of a cavity as spherical is justified provided the ratio of length to diameter of explosive does not exceed 6. A long charge with a ratio over 6 may be divided into two subcharges placed at 1/4 charge lengths away from its two ends. Each of the two subcharges has half of the total weight of the long charge and may be modelled the same way as a single charge using the idealized model.

The idealized model assumes the medium to be homogeneous and infinite. This assumption excludes consideration of reflections and refractions of waves at elastic discontinuities, and it does not simulate the change of waveforms near the ground surface (free surface effects) in an actual detonation. The idealized model discussed in the present chapter also assumes the medium to be linear elastic. This assumption does not include the significant effects of fracturing, crushing, and shear failure of materials surrounding the cavity, and also the important contribution of the viscosity and frictional resistance of the medium on wave propagation from the blast point.

2.2 The 3D Spherically Symmetric Finite Element Formulation

A finite element formulation is presented for dynamic analysis of the idealized model in the time domain. Dynamic response of the elastic medium is obtained using the general three dimensional (3D) wave equation with simplification to spherically symmetric conditions. This is found to be a useful starting point in model development due to the fact that three spatial coordinates are reduced to one (radial distance from the blast point), resulting in considerable reduction in computational effort. At a later stage of research, it may be useful to extend the model to consider axially symmetric response in which free surface effects are considered.

2.2.1 3D Dynamic Equations

In a 3D space xyz, displacements in the x, y, and z coordinate directions are represented by u, v and w, respectively. The normal strain components ε_x, ε_y, ε_z and the shear strain components γ_{xy}, γ_{yz} γ_{zx} in the 3D space are commonly expressed in terms of displacements as

$$\varepsilon_x = \frac{\partial u}{\partial x} ; \qquad \varepsilon_y = \frac{\partial v}{\partial y} ; \qquad \varepsilon_z = \frac{\partial w}{\partial z} \tag{1}$$

$$\gamma_{xy} = \frac{\partial v}{\partial x} + \frac{\partial u}{\partial y} \tag{2}$$

$$\gamma_{yz} = \frac{\partial w}{\partial y} + \frac{\partial v}{\partial z} \tag{3}$$

$$\gamma_{zx} = \frac{\partial w}{\partial x} + \frac{\partial u}{\partial z} \tag{4}$$

Equations (1) to (4) are valid under small strain conditions. The 3D undamped wave equations governing the free vibration response of an elastic medium are written as

$$\rho\frac{\partial^2 u}{\partial t^2} = (\lambda + G)\frac{\partial(\varepsilon_x+\varepsilon_y+\varepsilon_z)}{\partial x} + G(\frac{\partial^2 u}{\partial x^2}+\frac{\partial^2 v}{\partial y^2}+\frac{\partial^2 w}{\partial z^2}) \tag{5}$$

$$\rho\frac{\partial^2 v}{\partial t^2} = (\lambda + G)\frac{\partial(\varepsilon_x+\varepsilon_y+\varepsilon_z)}{\partial y} + G(\frac{\partial^2 u}{\partial x^2}+\frac{\partial^2 v}{\partial y^2}+\frac{\partial^2 w}{\partial z^2}) \tag{6}$$

$$\rho\frac{\partial^2 w}{\partial t^2} = (\lambda + G)\frac{\partial(\varepsilon_x+\varepsilon_y+\varepsilon_z)}{\partial z} + G(\frac{\partial^2 u}{\partial x^2}+\frac{\partial^2 v}{\partial y^2}+\frac{\partial^2 w}{\partial z^2}) \tag{7}$$

where
G = shear modulus of elastic medium
λ = Lame's constant, $\lambda = B - 2/3 * G$
B = bulk modulus of the elastic medium
ρ = mass density of the elastic medium

$V_p = 1430$ m/s for water (pg 27)

The shear wave velocity V_S and the compressive wave velocity V_P are related to these parameters as

$$V_s = \sqrt{\frac{G}{\rho}} \quad and \quad V_p = \sqrt{\frac{B + 4/3\ G}{\rho}} \tag{8}$$

The Poisson's ratio μ of the elastic medium is related to the shear modulus G and bulk modulus B as

$$\mu = \frac{3B - 2G}{6B + 2G} \tag{9}$$

2.2.2 Finite Element Method

In the finite element method, the displacement components are directly computed at each nodal point. The displacements at any point within a finite element domain are evaluated from these nodal displacements $\delta_i = (u_i, v_i, w_i)^T$ using shape functions $N_i(x,y,z)$. For a finite element of n nodes, the following relationship exists

$$\delta(x,y,z) = \Sigma\ N_i(x,y,z)\ \delta_i \qquad i = 1, n \tag{10}$$

Using equations (1) to (4), the 3D strain components $\{\varepsilon\}$ can be determined from the nodal displacements δ as follows

$$\{\varepsilon\} = [B]\ \{\delta\} \tag{11}$$

where
$[\varepsilon] = \{ \varepsilon_x, \varepsilon_y, \varepsilon_z, \gamma_{xy}, \gamma_{yz}, \gamma_{zx} \}^T$
$\{\delta\} = \{ \delta_1, \delta_2, \delta_3, \ldots, \delta_n\}^T$
$[B]$ = strain - displacement matrix

The strain-displacement matrix [B] consists of first derivatives of shape functions N_i. The detailed expression for [B] matrix can be found in text books describing the general theory of the finite element method (Cook et al., 1989).

The stress vector $\{\sigma\}$ can be computed from the strain vector $\{\varepsilon\}$ using the linear elastic stress-strain relationship as

$$[\sigma] = [D]\ \{\varepsilon\} \tag{12}$$

where $[\sigma] = \{\ \sigma_x,\ \sigma_y,\ \sigma_z,\ \tau_{xy}, \tau_{yz}, \tau_{zx}\ \}^T$

[D] is the elastic stress-strain matrix

The [D] matrix is defined in terms of shear modulus G and Lame's constant λ as

$$[D] = \begin{bmatrix} D_{11} & 0 \\ 0 & D_{22} \end{bmatrix} \tag{13}$$

and

$$[D_{11}] = \begin{bmatrix} \lambda+2G & \lambda & \lambda \\ \lambda & \lambda+2G & \lambda \\ \lambda & \lambda & \lambda+2G \end{bmatrix} \tag{14}$$

$$[D_{22}] = \begin{bmatrix} G & 0 & 0 \\ 0 & G & 0 \\ 0 & 0 & G \end{bmatrix} \tag{15}$$

Applying the general procedures for a finite element method, the 3D wave equations for free vibrations described by equations (5) to (7) are discretized into matrix form as

$$[M]\{\frac{\partial^2 \delta}{\partial t^2}\} + [K]\{\delta\} = \{0\} \tag{16}$$

where [M], [K] are the global mass matrices and stiffness matrices, respectively, and they are assembled from the mass matrix $[M]_{elem}$ and stiffness matrix $[K]_{elem}$ of each element. These matrices are determined for each element using the following integration over the volume of the finite element

$$[M]_{elem} = \int_v \rho \; [N_i] \; [N_j] \; dv \tag{17}$$

$$[K]_{elem} = \int_v [B]^T \; [D] \; [B] \; dv \tag{18}$$

For a damped system with a damping matrix [C] subjected to forced vibration by an external transient force {F(t)}, the discretized equations of motion are written as

$$[M]\{\frac{\partial^2 \delta}{\partial t^2}\} + [C]\{\frac{\partial \delta}{\partial t}\} + [K]\{\delta\} = \{F(t)\} \tag{19}$$

2.2.3 Finite Element Formulation - 3D Spherically Symmetric Model

For the mechanical model used, spherically symmetric conditions are applicable which reduce the field variables from three displacement components to one single displacement component. In a 3D spherical coordinate system, the displacement in the radial direction is u_r. The two tangential displacements u_θ and u_ϕ are zero. The shear stresses and shear strains in the radial and the two tangential directions are also zero in the 3D spherical coordinate system. However normal strains and stresses do exist and are determined by

$$\varepsilon_r = \frac{\partial u_r}{\partial r} \tag{20}$$

$$\varepsilon_\theta = \varepsilon_\phi = \frac{u_r}{r} \tag{21}$$

$$\sigma_r = (\lambda + 2G)\varepsilon_r + \lambda\varepsilon_\theta + \lambda\varepsilon_\phi \tag{22}$$

$$\sigma_\theta = \lambda\varepsilon_r + (\lambda+2G)\varepsilon_\theta + \lambda\varepsilon_\phi \tag{23}$$

$$\sigma_\phi = \lambda\varepsilon_r + \lambda\varepsilon_\theta + (\lambda+2G)\varepsilon_\phi \tag{24}$$

A 3-node quadratic line element is used to model the dynamic displacement in the radial direction u_r. The quadratic variation of the displacement u_r within each finite element is shown in Figure 2.2. The shape functions for this element are given as

$$N_1(\xi) = \frac{2}{L^2}(\xi^2-1.5L\xi+0.5L^2) \tag{25}$$

$$N_2(\xi) = -\frac{4}{L^2}(\xi^2-L\xi) \tag{26}$$

$$N_3(\xi) = \frac{2}{L^2}(\xi^2-0.5L\xi) \tag{27}$$

where ξ is the local axis with $\xi = 0$ at node 1 and $\xi = L$ at node 3 as shown in Figure 2.2. The 3-node quadratic element gives a quadratic variation of displacement and a linear variation of strains and stresses with each finite element. The displacement modes are also shown in Figure 2.2.

The element mass matrix and the stiffness matrix are computed using equations (14) and (15) with $dv=4\pi r^2 dr$, respectively. The detailed formulations of these matrices are given in appendix I.

The global equations governing the undamped motions of the idealized model subjected to transient force {F(t)} are given in matrix form as

$$[M]\{\frac{\partial^2 u_r}{\partial t^2}\} + [K]\{u_r\} = \{F(t)\} \tag{28}$$

where [M], [K] are the global mass matrices and stiffness matrices, respectively, and F(t) is determined from the dynamic pressure as $\{F(t)\} = 4\pi a^2\{p(t)\}$. Section 2.3 gives the magnitude and the form of dynamic pressure {p(t)} which acts on the surface of the cavity.

half used in code. also half stiffness & mass matrix [illegible]

Dynamic analyses are conducted in the time domain using the Wilson-θ step-by-step integration method (Clough and Penzien, 1975; Wilson et al., 1973). A coefficient $\theta = 1.4$ to 1.5 is used in the analyses.

The following section gives the magnitude and the form of dynamic pressure $\{p(t)\}$ which acts on the surface of the cavity.

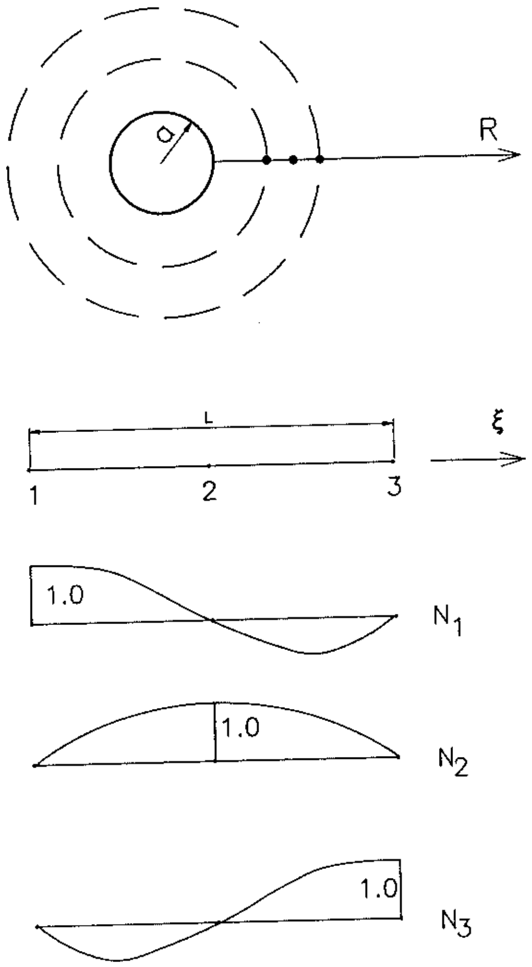

Figure 2.2 Characteristics of the Quadratic 3-Node Finite Element

2.3 Transient Dynamic Borehole Pressures due to Detonation of Explosives

The peak detonation pressure of a specific explosive, i.e., the peak dynamic pressure acting at the cavity surface, is given by the U.S. Army Corps of Engineers (1972) as

$$P_0 = 6.06\times10^{-3}(\frac{\rho_e V_d^2}{1+0.8\rho_e}) \tag{29}$$

where P_0 = peak detonation pressure (psi)
V_d = detonation velocity of the explosive (ft/sec)
ρ_e = specific gravity of the explosive (g/cm^3)

or in metric units (P_0 in kPa; V_d in m/sec; ρ_e in g/cm^3)

$$P_0 = 450.0\times10^{-3}(\frac{\rho_e V_d^2}{1+0.8\rho_e}) \tag{30}$$

Using a Dynamite with ρ_e=1.3 g/cm^3 and V_d=19,000 ft/sec (5,793 m/sec) produces a detonation pressure of approximately 1.4 x 10^6 psi (9.75 x 10^6 kPa). Using a Tovex explosive with ρ_e = 1.18 g/cm^3 and V_d=15,744 ft/sec (4,800 m/sec) generates a detonation pressure of about 0.91 x 10^6 psi (6.29 x 10^6 kPa) at the borehole casing.

Usually the dynamic borehole pressure rises very rapidly, achieving its peak within 1 millisecond (1 ms = 10^{-3} sec) and then decays exponentially with time as schematically shown in Figure 2.3. A combination of two exponential functions is assumed to represent the time variation of dynamic borehole pressure

$$p(t)=A\ (e^{-\alpha t}-e^{-\beta t}) \tag{31}$$

where A, α, β are constants. A controls the peak value of p(t) and α and β control the shape of p(t).

The rise time t_p of the pressure pulse and the peak dynamic pressure P_0 are determined by

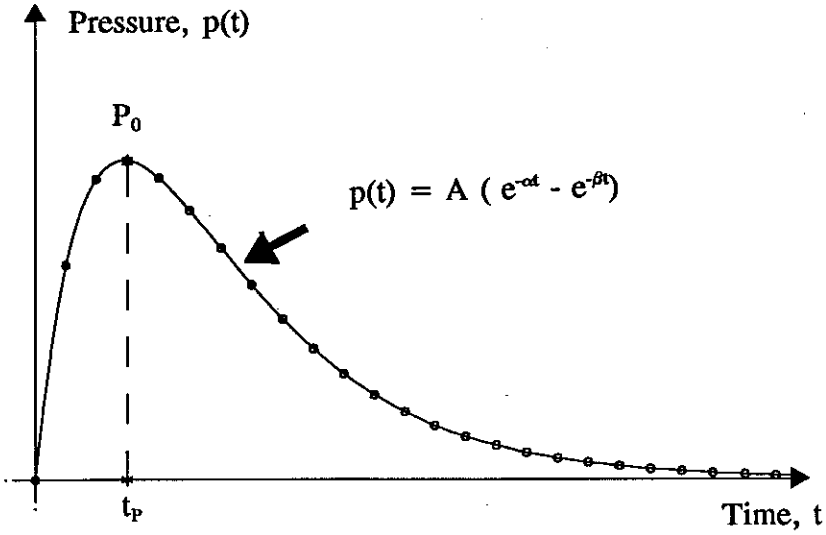

Figure 2.3 Input Dynamic Pressure on the Cavity Surface

$$t_p = \frac{\ln(\beta/\alpha)}{\beta-\alpha} \tag{32}$$

$$P_0 = A\ (e^{-\alpha t_p} - e^{-\beta t_p}) \quad or \quad A = \frac{P_0}{(e^{-\alpha t_p} - e^{-\beta t_p})} \tag{33}$$

For a selected shape of dynamic pressure with known α and β, and a peak dynamic pressure P_0 determined for a given explosive from equation (29), the shape of the pressure-time function is determined from equation (31). Figure 2.4 shows configurations of dynamic pressures for different combinations of α and β for a peak pressure of P_0 = 337,440 kPa.

A combination of α=1000 and β=2000 gives a rise time of t_p=0.69 ms. This combination is selected for describing dynamic pressure acting at the surface of the spherical cavity unless indicated otherwise.

In the analyses presented, dynamic pressures are assumed to vary with types of explosive but they are considered to be independent of the charge weight. The charge weight W determines the radius of the spherical cavity using the following equation

$$W = \frac{4}{3}\pi a^3 \rho_e \quad or \quad a = (\frac{3W}{4\pi\rho_e})^{0.3333} \tag{34}$$

A heavier charge will produce a larger cavity and therefore deliver more energy to its surrounding medium.

The magnitude and the form of the dynamic pressure induced by the explosive detonation have great influence on the outcome of a dynamic analysis. Research is still required in this area to obtain a more representative time history of this dynamic pressure.

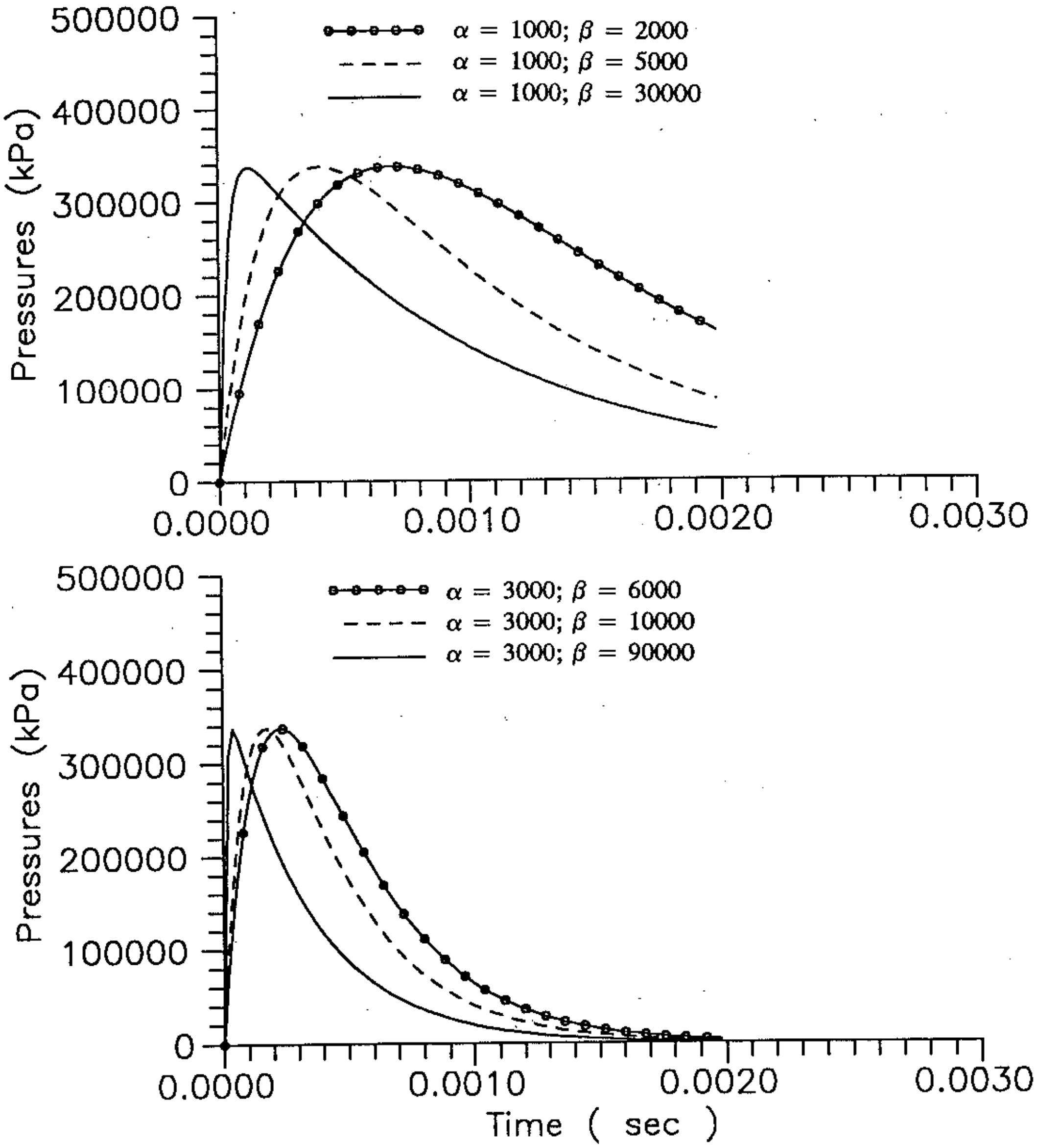

Figure 2.4 Configuration of Dynamic Pressures for Different Combinations of α and β

2.4 Sharpe's (1942) Analytical Solutions

Sharpe (1942) presented analytical solutions to the mechanical model shown in Figure 2.1 subjected to a dynamic pressure of the form $p(t) = P_0 e^{-\alpha t}$. Using the spherically symmetric conditions the 3D wave equations (5) to (7) are reduced to a spherical wave equation.

The spherical wave equation governing the dynamic response of the elastic medium around the cavity is given by

$$(\lambda + 2G)\left(\frac{\partial^2 \phi}{\partial r^2} + \frac{2}{r}\frac{\partial \phi}{\partial r}\right) = \rho \frac{\partial^2 \phi}{\partial t^2} \tag{35}$$

where ϕ = displacement potential
t = time

The radial displacement u_r along the radial direction of a charge is determined from the displacement potential ϕ by $u_r = \partial\phi / \partial r$.

Applying boundary condition, $\sigma_r(r=a) = -p(r,t)_{r=a} = -P_0\, e^{-\alpha t}$, solutions to equation (35) were found by Sharpe as

$$\phi = \frac{P_0 a}{\rho[\omega_0^2 + (\alpha_0 - \alpha)^2]}\left[e^{-\alpha_0 T}\cos(\omega_0 T) + \frac{\alpha_0 - \alpha}{\omega_0}\sin(\omega_0 T) - e^{-\alpha T}\right] \tag{36}$$

where $\alpha_0 = V_P(1-2\mu)/(1-\mu)/a$
$\omega_0 = V_P(1-2\mu)^{0.5}/(1-\mu)/a$
$T = t - (r-a)/V_P$

Expressions of dynamic displacement u_r, particle velocity, acceleration and the various strain components are given in Appendix II. A computer program has been written for computing the dynamic response of the elastic medium using Sharpe's analytical solutions. The source code of the program is listed in Appendix II.

The solution to a cavity pressure of the form $p(t) = P_0(e^{-\alpha t} - e^{-\beta t})$ is then obtained by superposition of two separate solutions for pressure variations $p(t) = P_0 e^{-\alpha t}$ and $p(t) = P_0 e^{-\beta t}$. The form of the complete function ϕ can be established by replacing α by β in equation (36) and subtracting the resulting expression from that given in equation (36). Other field variables such as displacement, velocity, acceleration, and strain can be obtained using the same superposition technique.

2.5 Comparison Between Finite Element Solutions and Sharpe's Solution

Table 2.1 presents the parameters of a mechanical model that is used for verifying the finite element method against Sharpe's analytical elastic solutions. A one-dimensional mesh of 999 nodes and 499 elements (Mesh A) is used in the finite element analysis. The detailed mesh is shown in Figure 2.5. In the mesh each element zone is described by the number of elements and the length (m) of the constant length element in the form such as 50 @ 0.10 . A time increment of Δt=5.0E-6 sec is used in the step-by-step dynamic integration.

Table 2.1 Parameters Used in the Verification Analysis

shear modulus $G = 64{,}000$ kPa
bulk modulus $B = 5{,}623{,}511$ kPa
mass density $\rho = 2.0$ g/cm^3
cavity radius $a = 0.025$ m
constants defining input dynamic pressure in equation (28)
$\alpha = 1000$; $\beta = 30{,}000$; $A = 1.35E+6$ kPa

Results from the finite element analysis agree very well with those obtained from Sharpe's analytical solutions as shown in Figure 2.6, 2.7 and 2.8. Figure 2.6 shows a comparison of peak dynamic radial displacement with radial distance from the cavity. Figure 2.7 and Figure 2.8 give comparisons of the time variation of displacement and radial stress at a distance $r = 6.08$ m away from the cavity surface.

Elastic waves travel away from the source of dynamic pressure and their amplitudes decay with radial distance because of geometric (or radiation) damping. The decay of response amplitude with distance is also illustrated in Figure 2.9. The arrival times of the elastic wave at points r=3.0 m and r=6.08 m away from the source are clearly captured by the finite element analysis as shown in the figure. Times required for an elastic wave of V_P = 1689.5 m/sec to travel 3.0 m and 6.08 m are 1.78 ms and 3.60 ms, respectively, which agree well with those from the finite element analysis.

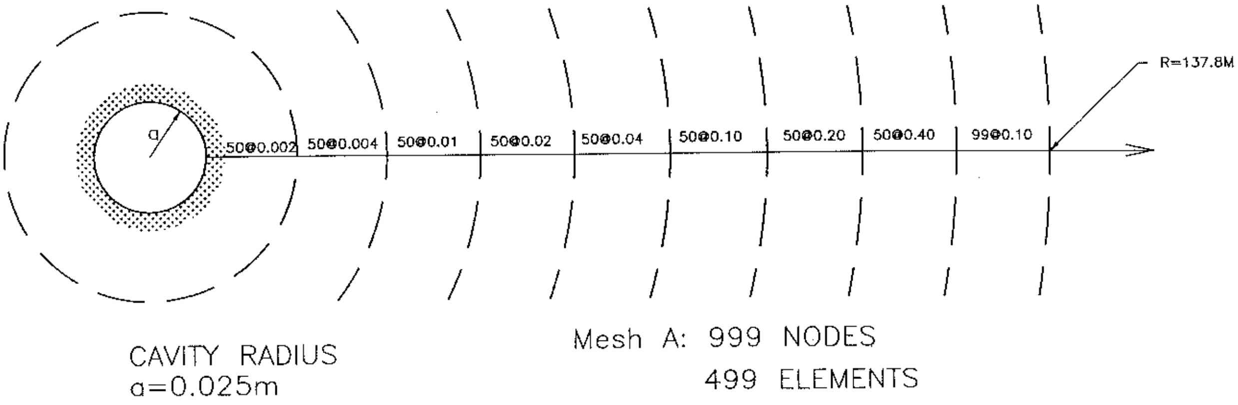

Figure 2.5 The finite element grid in Mesh A

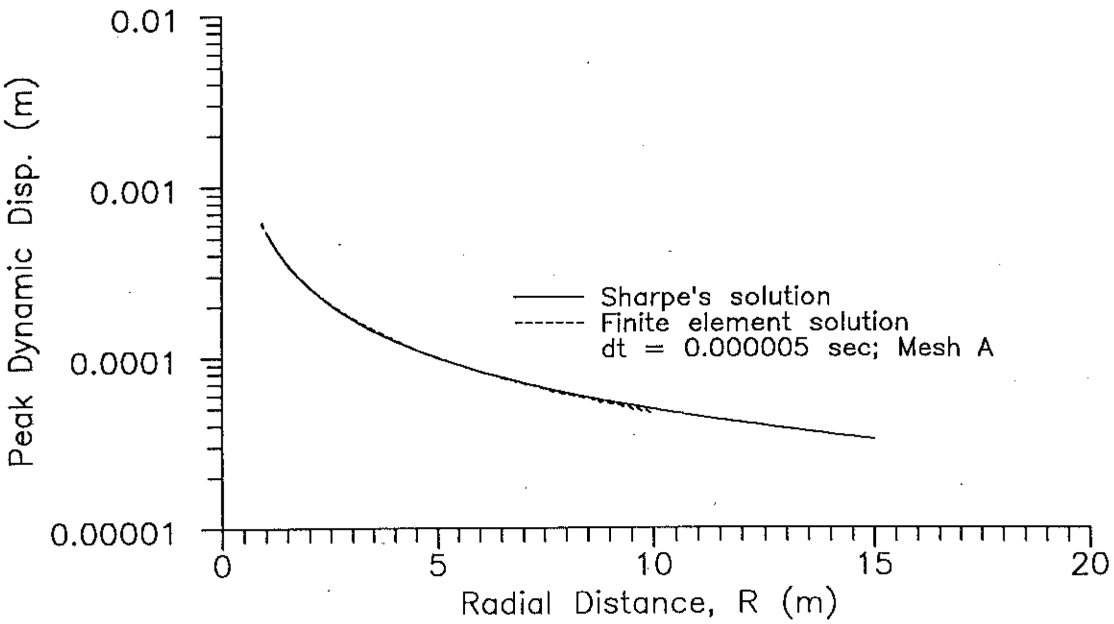

Figure 2.6 Computed Peak Dynamic Displacements versus Radial Distance

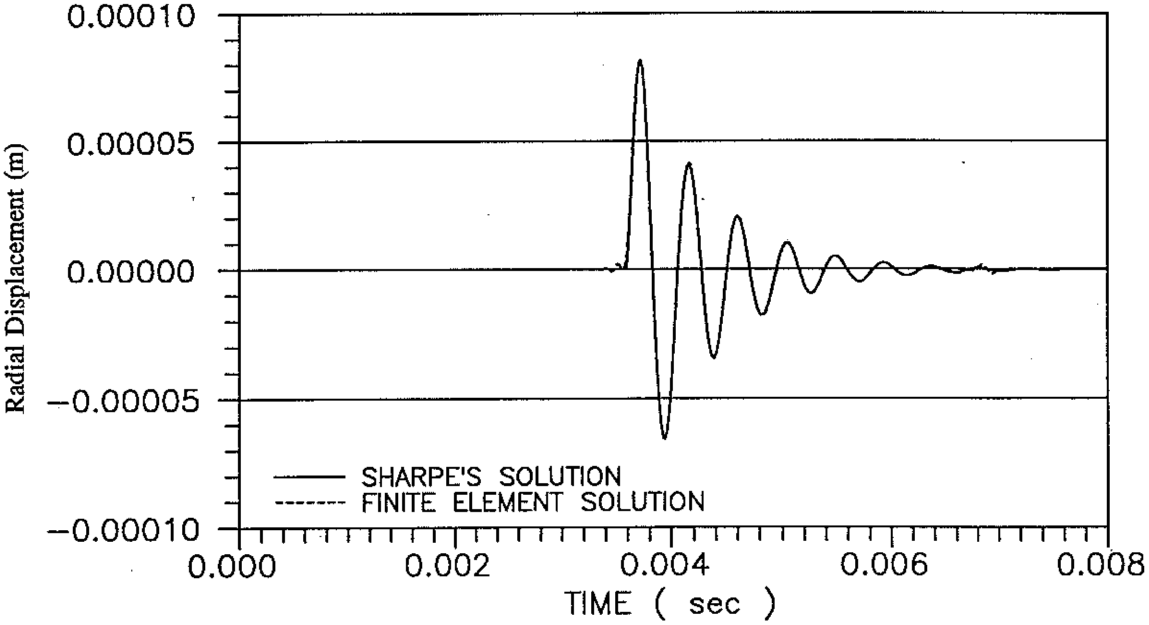

Figure 2.7 Computed Displacement Response at r = 6.08 m

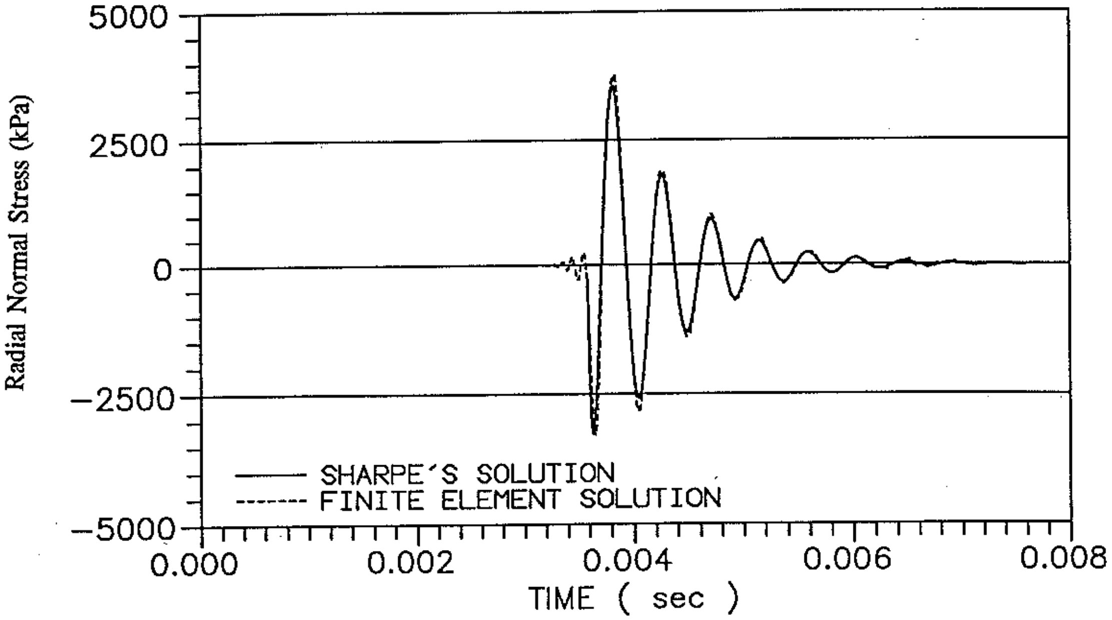

Figure 2.8 Computed Radial Stress Response at r = 6.08 m

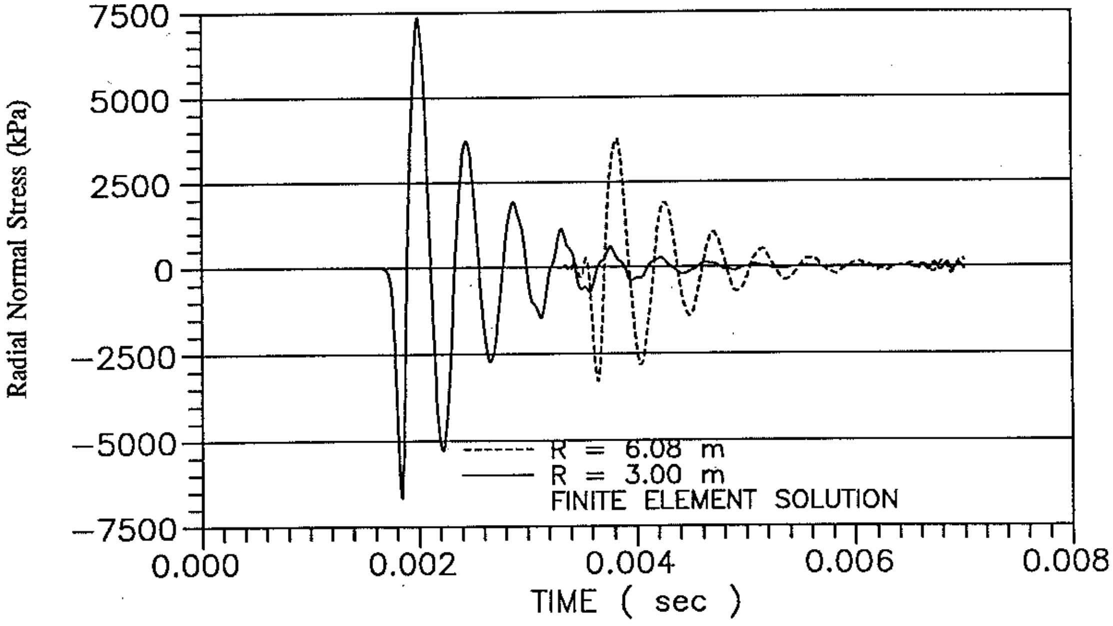

Figure 2.9 Computed Radial Stress Response at r = 3.0 m and at r = 6.08 m

2.6 Effects of Mesh Grid and Integration Time Increment Δt

Under linear elastic conditions, a fine mesh and a small integration time increment must be used in order to obtain accurate solutions using the finite element analysis.

Another mesh of 699 nodes and 349 elements has been used to study the effect of mesh grid on dynamic response. The finite element grid of this mesh (Mesh D) is shown in Figure 2.10. The peak dynamic displacements versus radial distance computed using Mesh D are compared in Figure 2.11 to those from analyses using Mesh A having 999 nodes. The comparison shows that the use of a coarser mesh (Mesh D) significantly underpredicts peak dynamic displacements.

Another study was conducted to examine the effect of integration time increment Δt on dynamic response. A larger Δt = 2.0E-5 sec with the fine mesh (Mesh A) was used. Computed dynamic displacements at radial distances r = 3.0 m and r = 6.08 m are shown in Figure 2.12. The comparison of solutions using Δt = 5.0E-6 sec and Δt = 2.0E-5 sec shows that the use of a larger Δt results in a stiffer system and therefore underpredicts the dynamic displacement at a given radial distance.

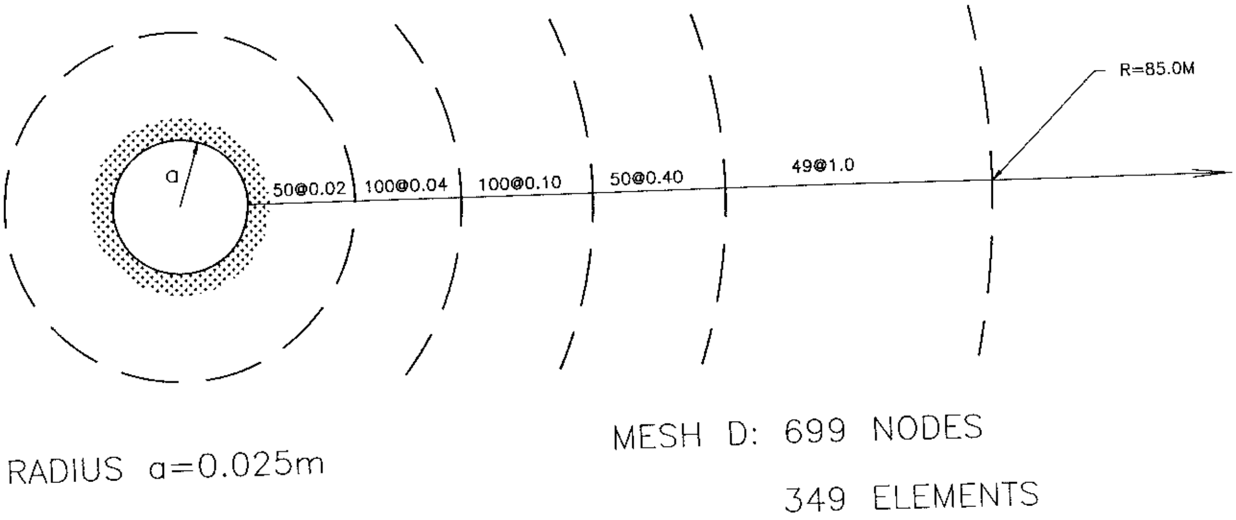

Figure 2.10 The Finite Element Grid in Mesh D

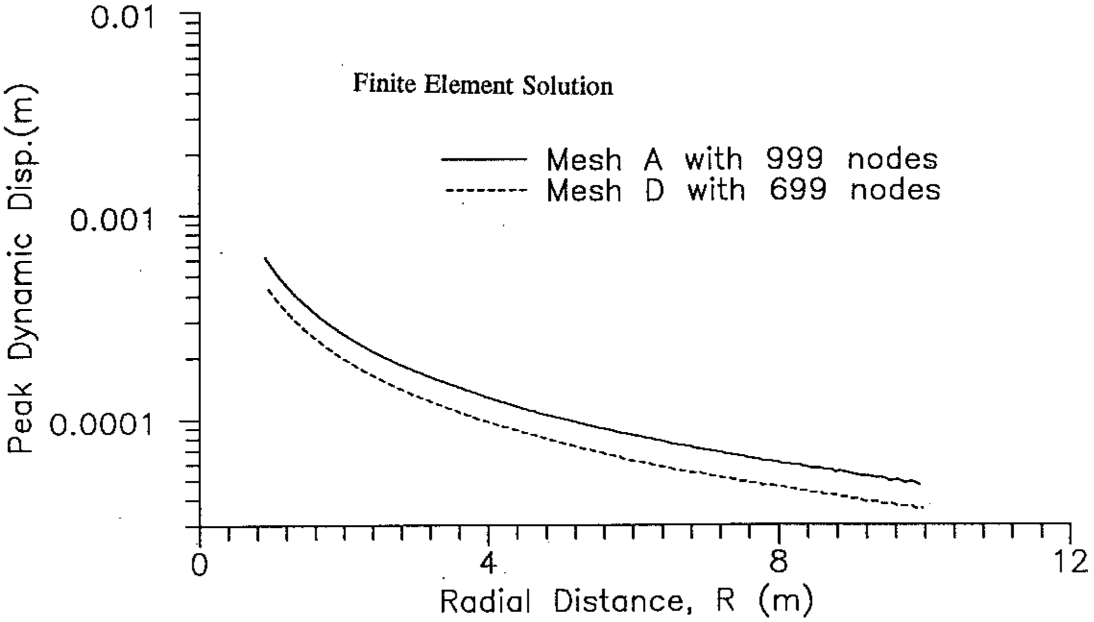

Figure 2.11 Computed Peak Dynamic Displacement Using Mesh A and Mesh D

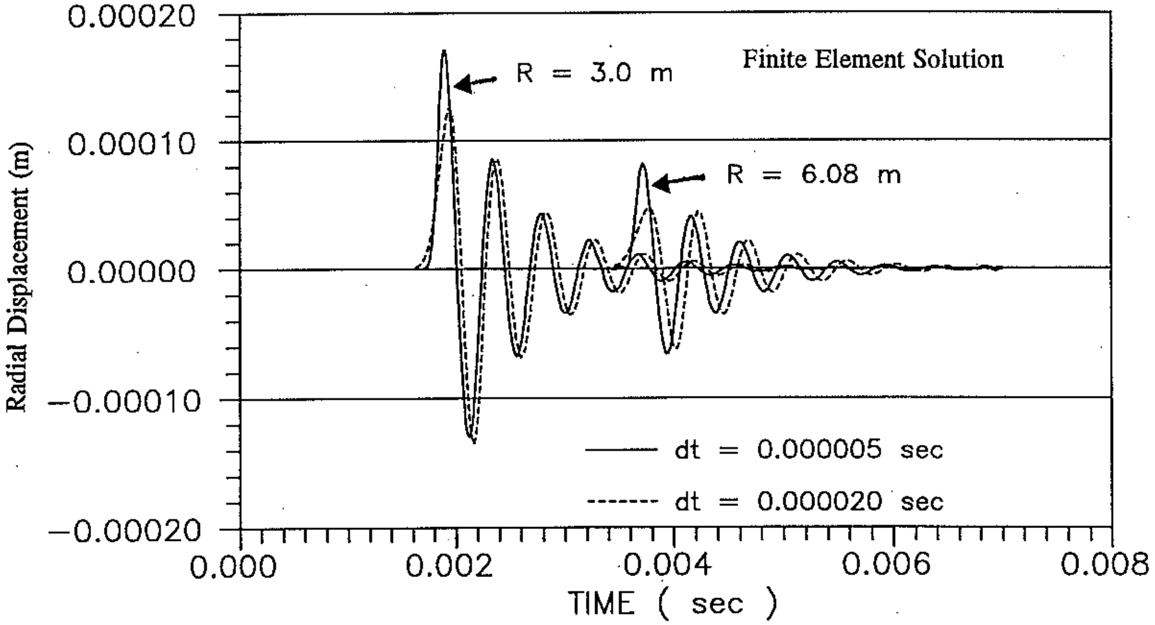

Figure 2.12 Computed Displacements at r = 3.0 m and r = 6.0 m Using Δt=2.0E-5 sec and Δt=5.0E-6 sec

3.0 NONLINEAR DYNAMIC RESPONSE OF SATURATED GRANULAR SOILS SUBJECTED TO BLAST LOADS

In this chapter the dynamic response of saturated granular soils are simulated using the 3D spherically symmetric finite element formulation described in the previous chapter. Saturated granular soils exhibit nonlinear and viscous behaviour during blast loading. In the numerical model, the nonlinear behaviour of the soil shear stress-shear strain relationship is modelled using an incremental elastic approach. The model is constructed to follow a loading-unloading hysteresis loop as a soil element undergoes shear straining. Soil-water viscosity is also included to simulate the dependence of the shear resistance of soil, especially saturated soil, to the time rate of shear strain. It has been found that these features of the numerical model successfully capture the basic features of saturated soil response to blast loads.

3.1 Modelling of Strain-Stress Behaviour

In the numerical model the relationship between the shear strain γ and the shear stress τ is modelled as nonlinear and hysteretic.

Under 3D spherically symmetric conditions, the shear strain γ is defined to be the difference between the radial normal strain ε_r and the tangential normal strain ε_θ as

$$\gamma = \varepsilon_r - \varepsilon_\theta \tag{37}$$

and the shear stress τ is defined by the radial normal stress σ_r and the tangential normal stress σ_θ as

$$\tau = \frac{\sigma_r - \sigma_\theta}{2} \tag{38}$$

To simplify the computations, the stress-strain curve at each Gauss point within a finite element is assumed to follow the hyperbolic loading - unloading - reloading relationships defined using an extended Masing criterion (Lee, 1975; Finn et al., 1977 and Finn et al., 1986). The hyperbolic curve is defined by two fundamental parameters which are the shear strength $\tau_{\max}$ and the in-situ low strain shear modulus $G_{\max}$ as shown in Figure 3.1.

The shear stress-strain backbone curve for describing the initial loading is defined by the following equation

$$\tau = \frac{G_{max} \cdot \gamma}{1 + \frac{G_{max}}{\tau_{max}} \cdot |\gamma|} \tag{39}$$

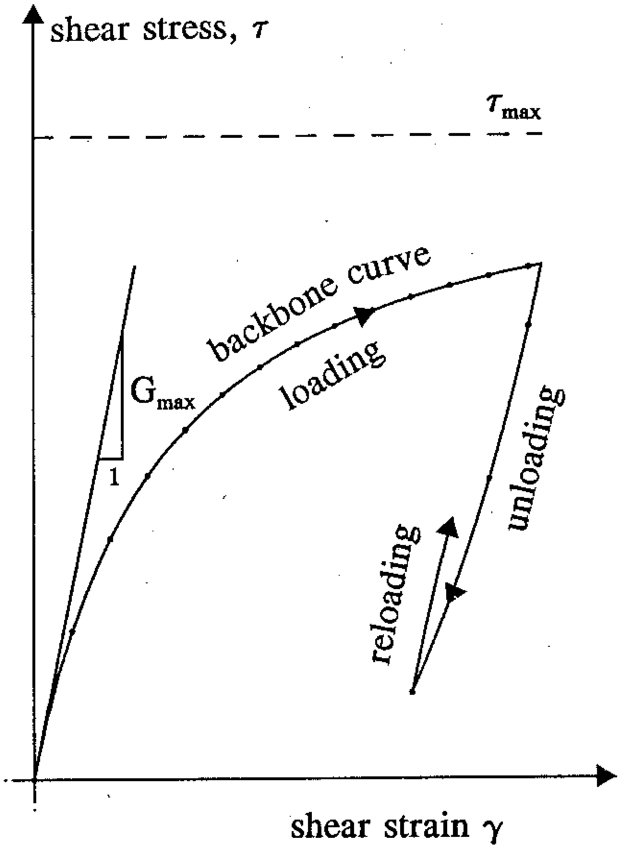

Figure 3.1 The modelling of hysteretic shear stress-strain behaviour

The strain response of the soil to a stress increment is controlled by the tangent shear and tangent bulkmoduli appropriate to the current state of the soil. The tangent shear modulus G_t corresponding to a strain level γ on the backbone curve is computed by

$$G_t = \frac{G_{\max}\gamma}{\left(1 + \frac{G_{\max}}{\tau_{\max}}|\gamma|\right)^2} \tag{40}$$

The secant shear modulus G_{sec} corresponding to a strain level γ_a on the backbone curve is determined by

$$G_{sec} = \frac{G_{\max}}{1 + \frac{G_{\max}}{\tau_{\max}}|\gamma|} \tag{41}$$

By following the hysteretic stress-strain loop, the hysteretic damping of soil is automatically included. The equivalent hysteretic damping ratio D implied in the hyperbolic model can be calculated by

$$D = \frac{4}{\pi}\left(1 + \frac{1}{|\gamma|\cdot\frac{G_{\max}}{\tau_{\max}}}\right)\left[1 - \frac{1}{|\gamma|\frac{G_{\max}}{\tau_{\max}}}\ln\left(1 + |\gamma|\frac{G_{\max}}{\tau_{\max}}\right)\right] - \frac{2}{\pi} \tag{42}$$

The response of the soil to uniform all-round pressure is assumed to be linearly elastic, and dependent on the bulk modulus B of the soil-water mixture. The bulk modulus B can be determined from the compressive and shear wave velocities V_P, V_S and the mass density ρ using equation (8). For saturated soil the bulk modulus B can also be determined using the following equation

$$B = \frac{1}{nC_w + (1-n)C_s} \tag{43}$$

where n = porosity of the soil
C_w = compressibility of water
C_s = compressibility of soil particles

5.1×10^{-7} (kPa)$^{-1}$ 0°C & 0 pressure
3.9×10^{-7} (kPa)$^{-1}$ 0°C & 100 MPa

Typical values for C_w and C_s are 48.93 x 10^{-6} m^2/kN and 2.752 x 10^{-6} m^2/kN (Ishihara, 1967), respectively. Since C_w and C_s are constants for a soil specimen, the value of bulk modulus B is mostly

8 8

$B_w = 2.1 \times 10^6$

$B_s = 36 \times 10^8$ kPa

controlled by the porosity n of the specimen. A loose saturated soil shows a low bulk modulus and a high compressibility, and a dense saturated soil shows the opposite.

The dynamic water pressure P is computed from the normal total stress increments using the pore water pressure formulation given by Skempton (1954)

$$P = \frac{1}{3} B_{skempton} (\sigma_r + \sigma_\theta + \sigma_\phi) \tag{44}$$

where $B_{skempton}$ = Skempton pore water pressure constant associated with the degree of saturation of the soil. For saturated soils $B_{skempton}$ = 1.0 is used while for unsaturated soils $B_{skempton}$ ranges between 0.0 and 1.0.

3.2 Modelling of Viscosity

Soil-water viscosity becomes very important during high strain events as caused by blasting. Viscosity is not usually taken into account in dynamic response analyses of soil under earthquake loading. This is mainly because the particle velocity of soil due to earthquake loading is small which results in a small magnitude of the time rate of shear strain. Therefore, the shear resistance due to the time rate of shear strain only accounts for a very small portion of the total shear resistance of the soil and is safely ignored in the analysis. Under blast loads, the viscosity of saturated granular soils is of critical importance to the dynamic soil response because of larger particle velocities.

The viscosity of saturated granular soils is modelled assuming that the viscous drag is of the Newtonian type, or that the shear stress due to viscosity is proportional to the time rate of shear strain. Assuming a coefficient of viscosity, η, this relationship is expressed as

$$\tau = \eta \cdot \frac{\partial \gamma}{\partial t} \tag{45}$$

in which τ and γ are the shear stress and the shear strain as defined previously in equations (37) and (38). The stress - strain relationships in equations (22) to (24) for the 3D spherically symmetric model is rewritten using bulk modulus B and shear modulus G as follows

$$\sigma_r = (B+\frac{4}{3}G)\varepsilon_r + (B-\frac{2}{3}G)\varepsilon_\theta + (B-\frac{2}{3}G)\varepsilon_\phi \tag{46}$$

$$\sigma_\theta = (B-\frac{2}{3}G)\varepsilon_r + (B+\frac{4}{3}G)\varepsilon_\theta + (B-\frac{2}{3}G)\varepsilon_\phi \tag{47}$$

$$\sigma_\phi = (B-\frac{2}{3}G)\varepsilon_r + (B-\frac{2}{3}G)\varepsilon_\theta + (B+\frac{4}{3}G)\varepsilon_\phi \tag{48}$$

Considering the viscosity analogy in equation (45) to the shear stress - strain relationship $\tau = G\,\gamma$, one finds that the stresses due to viscosity can be determined by replacing G by η, and strains by time rate of strains in equations (46) to (48) (Sharpe, 1967). Viscosity is only applicable to shear and thus bulk modulus B is set to zero in these equations.

$$\sigma_r^\eta = (\frac{4}{3}\eta)\frac{\partial\varepsilon_r}{\partial t} + (-\frac{2}{3}\eta)\frac{\partial\varepsilon_\theta}{\partial t} + (-\frac{2}{3}\eta)\frac{\partial\varepsilon_\phi}{\partial t} \tag{49}$$

$$\sigma_\theta^\eta = (-\frac{2}{3}\eta)\frac{\partial\varepsilon_r}{\partial t} + (\frac{4}{3}\eta)\frac{\partial\varepsilon_\theta}{\partial t} + (-\frac{2}{3}\eta)\frac{\partial\varepsilon_\phi}{\partial t} \tag{50}$$

$$\sigma_\phi^\eta = (-\frac{2}{3}\eta)\frac{\partial\varepsilon_r}{\partial t} + (-\frac{2}{3}\eta)\frac{\partial\varepsilon_\theta}{\partial t} + (\frac{4}{3}\eta)\frac{\partial\varepsilon_\phi}{\partial t} \tag{51}$$

or

$$\{\sigma^\eta\} = [D^\eta]\ \{\frac{\partial\varepsilon}{\partial t}\} \tag{52}$$

where $\{\sigma^\eta\} = \{\ \sigma_r^\eta,\ \sigma_\theta^\eta,\ \sigma_\phi^\eta\ \}^T$

$\{\partial\varepsilon/\partial t\ \} = \{\ \partial\varepsilon_r/\partial t,\ \partial\varepsilon_\theta/\partial t,\ \partial\varepsilon_\phi/\partial t\}^T$

$$[D^{\eta}] = \frac{2}{3}\eta \begin{bmatrix} 2 & -1 & -1 \\ -1 & 2 & -1 \\ -1 & -1 & 2 \end{bmatrix} \tag{53}$$

The damping matrix $[C]_{elem}$ due to viscosity is then expressed as

$$[C]_{elem} = \int_{v} [B]^{T} \, [D^{\eta}] \, [B] \; dv \tag{54}$$

The global equilibrium equations are written in matrix form as

$$[M]\{\frac{\partial^2 u_r}{\partial t^2}\} + [C]\{\frac{\partial u_r}{\partial t}\} + [K]\{u_r\} = \{F(t)\} \tag{55}$$

where [M], [C], [K] are the global mass matrices, damping matrices and stiffness matrices, respectively. These matrices are assembled over each finite element in the system.

3.3 Results of Analyses

The numerical model is capable of predicting dynamic accelerations, particle velocities and dynamic water pressures that a saturated soil element experiences as the shock wave from the blast passes through the element. The capability of the method is illustrated for dynamic response analyses of water, saturated loose sand and saturated dense sand. In the analysis the coefficient of viscosity η for each case is determined by fitting the computed response, typically particle velocity and dynamic pore water pressure, to the corresponding measured response. This back-analysis process reveals that for a specific medium, the coefficient of viscosity η increases as the charge weight W increases.

Charge weights of 0.1 kg, 0.5 kg, 1.0 kg, 2.0 kg, 4.0 kg and 8.0 kg are used in the numerical modelling to cover the range of charge weights typically used in explosive compaction projects. The TNT equivalent of the explosives is considered to have a detonation velocity of V_d = 5,800 m/sec, a density of ρ_e = 1.30 g/cm^3 and an energy rating of 1000 calories per gram. A combination of α = 1000 and β=2000 in equation (26) is used to compute the time history input of dynamic borehole pressures p(t).

Peak accelerations, peak particle velocities, peak dynamic water pressures, and peak strains are presented against the scaled distance $R/W^{0.333}$ (R = distance from the charge in m; W = TNT equivalent charge weight in kg).

3.3.1 Response of Water to Blast Loads

Cole (1948) gave an empirical equation for computing peak dynamic pressure in water due to blast loads. His equation was obtained according to field measurements of peak dynamic water pressure and this equation is written as

$$P = 52{,}000 \; (R/W^{0.333})^{-1.13} \tag{56}$$

where P = peak dynamic water pressure, kPa
R = radial distance from the charge, m
W = charge weight, kg

$V_p = 1430$ m/s. (see pg 23)

The dynamic response of water to blast loads is modelled using the numerical model presented. In this analysis, a bulk modulus B = 2.045 x 10^6 kPa and a mass density ρ = 1.0 g/cm^3 was used. A very low shear modulus G = 0.01 kPa and a shear strength τ_{max} = 0.1 kPa was used to simulate the low frictional shear resistance of water. The shear resistance of water to blasting is attributed mainly to viscosity. Table 3.1 summarizes the coefficients of viscosity used in the numerical modelling. The peak dynamic response versus the scaled distance is shown in Figure 3.2 to Figure 3.6.

The dynamic water pressure P is computed from the normal stresses σ_r and σ_θ using equation (44). The computed peak dynamic water pressure agrees well with that given by Cole for scaled distances less than 7.0 (Figure 3.2). Beyond this range, the peak pressure given by Cole is larger than that computed from the numerical model.

Typically at r = 4.0 m away from a charge of 1.0 kg, the numerical model predicts a peak dynamic water pressure of 10,500 kPa, a peak acceleration of 2000 g and a peak particle velocity of 8.0 m/sec. The corresponding shear strain and volumetric strain at r = 4.0 m are in the order of 0.7% and 0.50%, respectively. For the same charge, the level of shear strain approaches 1% at r = 2.0 m.

Table 3.1 Coefficients of Viscosity η Corresponding to Charge Weight W in Water

W (kg)	0.1	0.5	1.0	2.0	4.0	8.0
η (kPa.s)	7.0	13.0	17.0	22.0	28.0	35.0

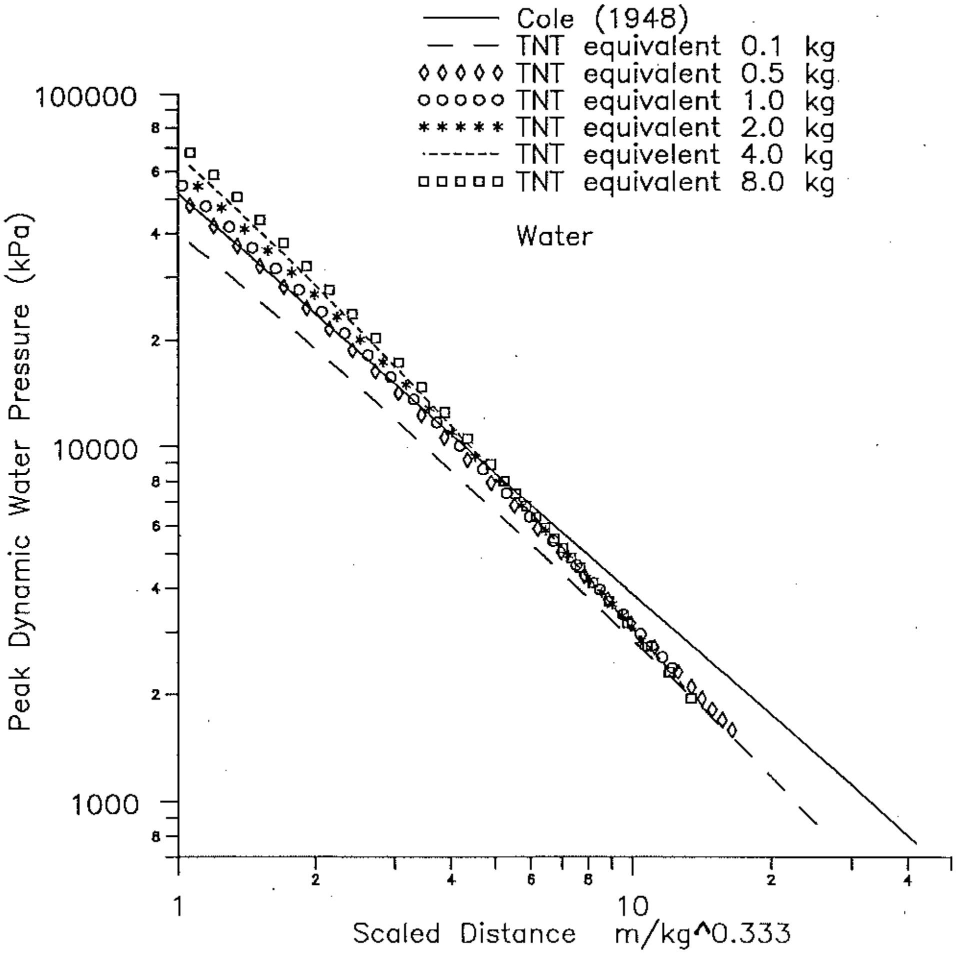

Figure 3.2 Computed Peak Dynamic Water Pressures vs. Scaled Distance $R/W^{0.333}$ in Water

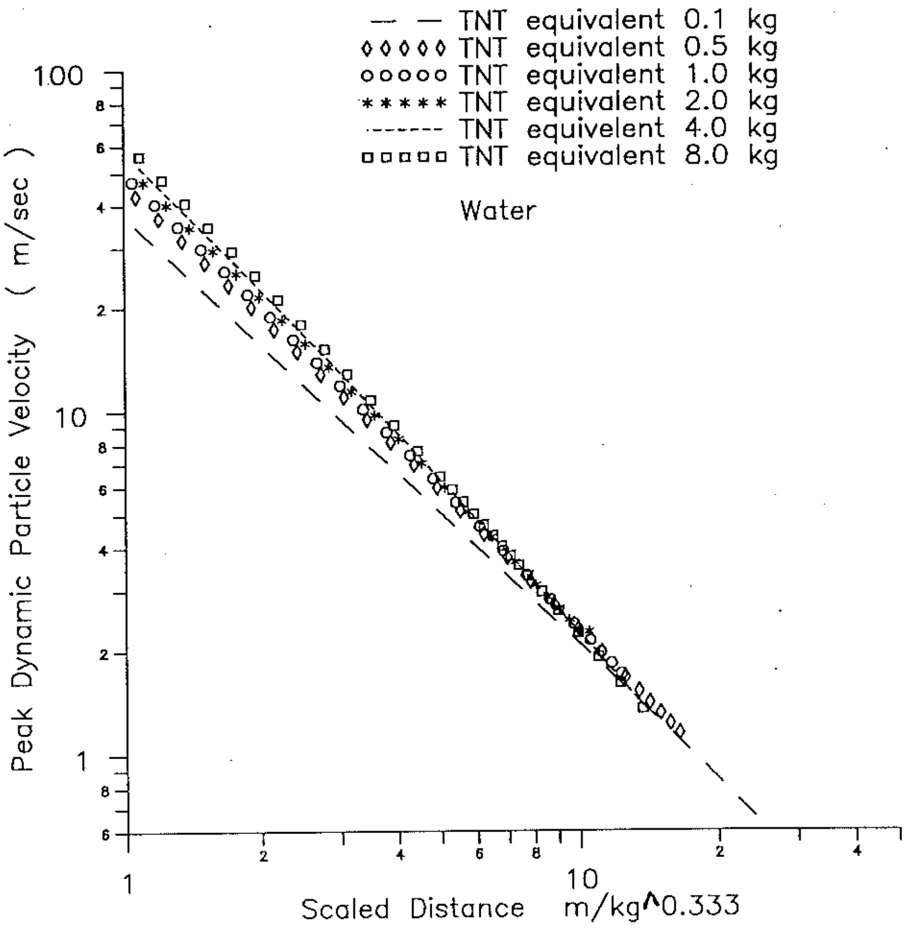

Figure 3.3 Computed Peak Particle Velocities vs. Scaled Distance $R/W^{0.333}$ in Water

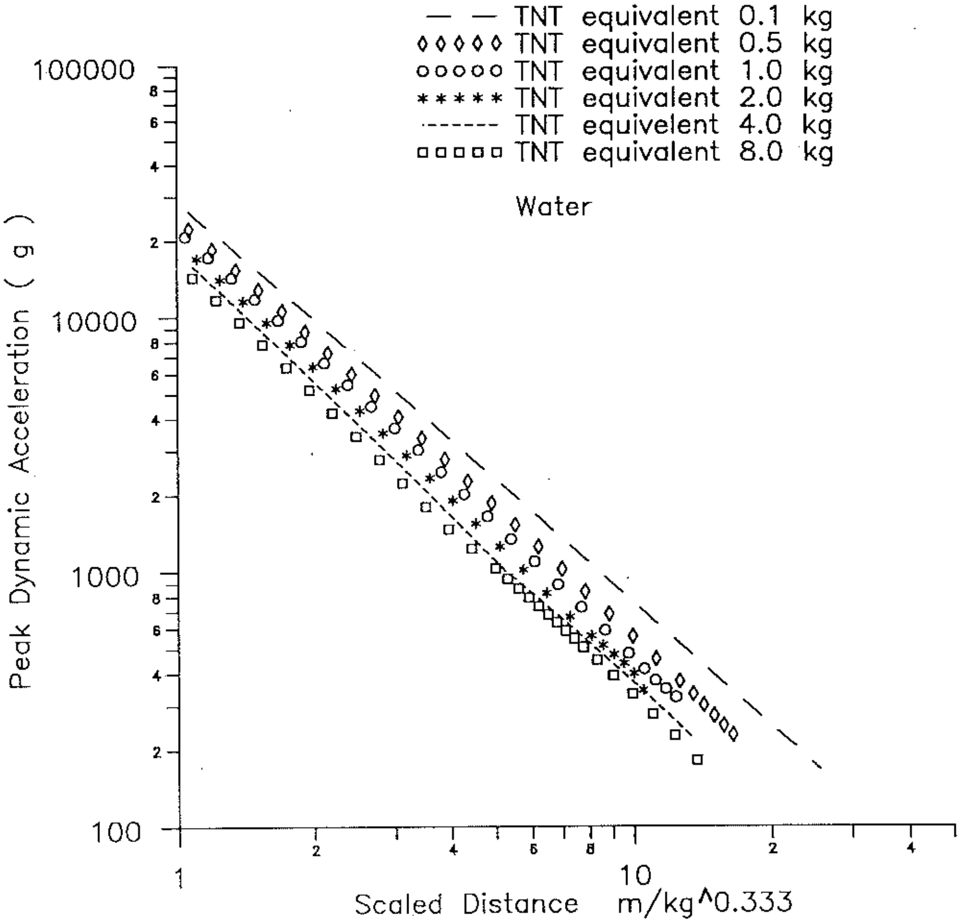

Figure 3.4 Computed Peak Accelerations vs. Scaled Distance R/$W^{0.333}$ in Water

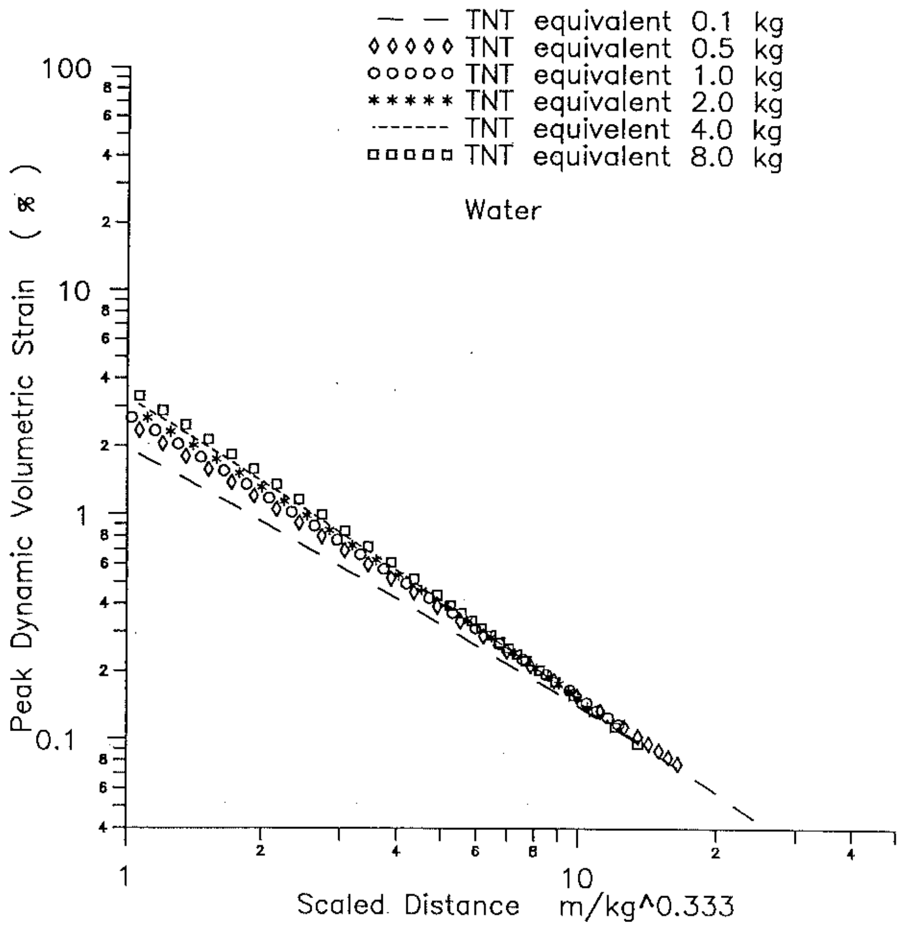

Figure 3.5 Computed Peak Dynamic Volumetric Strains vs. Scaled Distance $R/W^{0.333}$ in Water

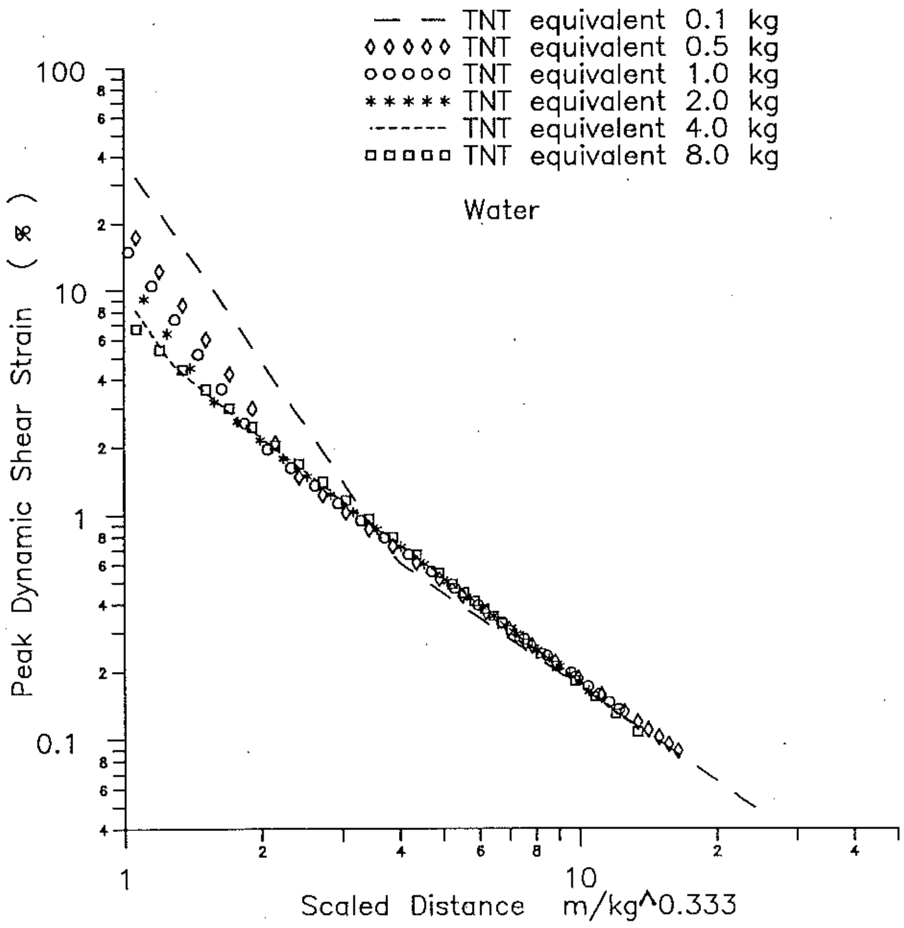

Figure 3.6 Computed Peak Dynamic Shear Strain vs. Scaled Distance R/W$^{0.333}$ in Water

3.3.2 Nonlinear Response of Saturated Loose Sand to Blast Loads

Test Results

Hryciw (1986) conducted a series of field blast tests in a saturated loose sand deposit. The tests consisted of a single charge at one test hole and of two or three decked charges at other test holes. Charges were located between 12 ft (3.6 m) to 24 ft (7.3 m) below the ground surface. Each charge contained a 3.8 lb (1.73 kg) dynamite having a detonation velocity of V_d = 5791 m/s. In the tests, peak dynamic water pressures and peak dynamic accelerations were measured 20 ft (6.1 m) below the ground surface, and at 20 ft (6.10 m) to 50 ft (15.2 m) away from the buried charges. The charge delays used during blasting, instrument locations relative to the charges, and measured peak dynamic responses are listed in Table 3.2.

Table 3.2 Peak dynamic water pressures and accelerations measured in a loose sand (charge per delay: 3.8 lb or 1.73 kg) (after Hryciw, 1986)

Delays (ms)	horizontal distance between charge and instrument (m)	hypocentral distance between charge and instrument (m)	peak acceleration (g)	peak water pressure (kPa)
S 0	first at 6.10 m	6.22	1194	4164
S 0	first at 12.2 m	12.44	269	738
A 0-0	first at 9.15 m	9.27	552	2606
A 0-0	second at 9.15 m	9.74	670	2027
A 0-0	first at 15.25 m	15.30	109	1406
A 0-0	second at 15.25 m	15.61	219	965
B 0-25	first at 9.15 m	9.27	1086	3730
B 0-25	second at 9.15 m	9.74	120	1214
B 0-25	first at 15.25 m	15.30	---	1855
D 0-25-50	first at 9.15 m	9.54	674	2503
D 0-25-50	second at 9.15 m	9.19	118	1489
D 0-25-50	third at 9.15 m	9.19	552	3158
D 0-25-50	first at 15.25 m	15.49	--	1903
D 0-25-50	second at 15.25 m	15.24	--	869
D 0-25-50	third at 15.25 m	15.24	--	1724

Peak particle velocities were recorded at the ground surface 50 ft (15.2 m) and 200 ft (61.0 m) away from the charges. The measured peak particle velocities are listed in Table 3.3.

Table 3.3 Peak particle velocities (m/sec) measured at the ground surface (charge per delay: 3.8 lb or 1.73 kg) (after Hryciw, 1986)

Delay (ms)	body wave at 15.24 m	body wave at 61.0 m	surface wave at 15.24 m	surface wave at 61.0 m
A 0-0	0.131	0.033	0.102	0.007
B 0-25	0.079	0.023	0.060	0.016

Hryciw (1986) reported that the ground consisted of loose sands having an average cone tip resistance Q_c = 2000 kPa to 3500 kPa and Standard Penetration blow counts of $(N_1)_{60}$ = 4 to 8. A compressive wave velocity of V_P = 5050 ft/sec (1540 m/s) was determined from the elapsed time that the shock wave travelled through a given distance in the loose sand.

Computed Dynamic Response for a Single Charge (W = 1.73 kg)

The above blast tests were modelled assuming single charge detonations and that the peak dynamic soil response from the detonation of one charge was reasonably unaffected by subsequent detonations. Dynamic response analyses have been performed using the test charge weight of W = 1.73 kg. In the analysis, the following properties of the saturated loose sand have been assumed: a shear wave velocity V_S = 150 m/s, a compressive wave velocity V_P = 1540 m/s, a saturated unit weight of 17 kN/m^3 and shear strength of τ_{max} = 35 kPa. The coefficient of viscosity η = 60 kPa.s was used for the analysis.

The computed time histories of dynamic particle displacement and acceleration at radial distances of r = 3.0 m and r = 6.1 m are shown in Figures 3.7 to 3.8 to illustrate typical dynamic response. A detailed comparison of computed and measured quantities is presented subsequently. After reaching their peak values, the computed dynamic displacements decay with time and exhibit a permanent residual displacement of about 3 mm at r =3.0 m and 0.6 mm at r =6.1 m, respectively. The computed particle accelerations experience a full cycle of vibration and decay to an "at rest" condition as the wave passes. Peak accelerations of 1200 g at r= 3.0 m and 400 g at r= 6.1 m are predicted from the analysis.

The computed normal stresses at r = 6.1 m are plotted with time in Figure 3.9. In the saturated loose sand, the radial normal stress σ_r and the tangential normal stress σ_θ or σ_ϕ ($\sigma_\theta = \sigma_\phi$ due to symmetry) are almost identical as can be seen from Figure 3.9. The dynamic water pressure P is computed from the normal stresses σ_r and σ_θ using equation (44) and $B_{skempton} = 1.0$. For the case presented here, dynamic pore water pressures are equivalent to normal stresses σ_θ or σ_r.

The computed results show the different response patterns for the radial and tangential normal strains. The radial strains are completely compressive while the tangential strains act in extension. The time history responses of the normal strain ε_r and the tangential strain ε_θ at r = 6.1 m are shown in Figure 3.10. The differences in computed normal and tangential strain indicate the significant shear strains generated by blast loads. The magnitude of shear strain γ in a soil element as defined previously in equation (37) is greater than the magnitude of volumetric strain ε_V of the element defined by

$$\varepsilon_V = \varepsilon_r + 2\ \varepsilon_\theta \qquad (57)$$

The computed shear strain γ and volumetric strain ε_V at r = 6.1 m are shown in Figure 3.11. The peak shear strain of the element is about 0.15%, and the peak volumetric strain of the same element is about 0.11%.

The hysteretic behaviour of a soil element simulated at r = 6.10 m in the numerical model is illustrated by the shear stress - shear strain loop shown in Figure 3.12. The shear stress is bounded by the shear strength of the soil $\tau_{max} = 35$ kPa. The shear stress - shear strain curve follows the backbone loading path when the shock front initially arrives at the soil element, and then undergoes unloading - reloading behaviour as the shock front passes by the soil element.

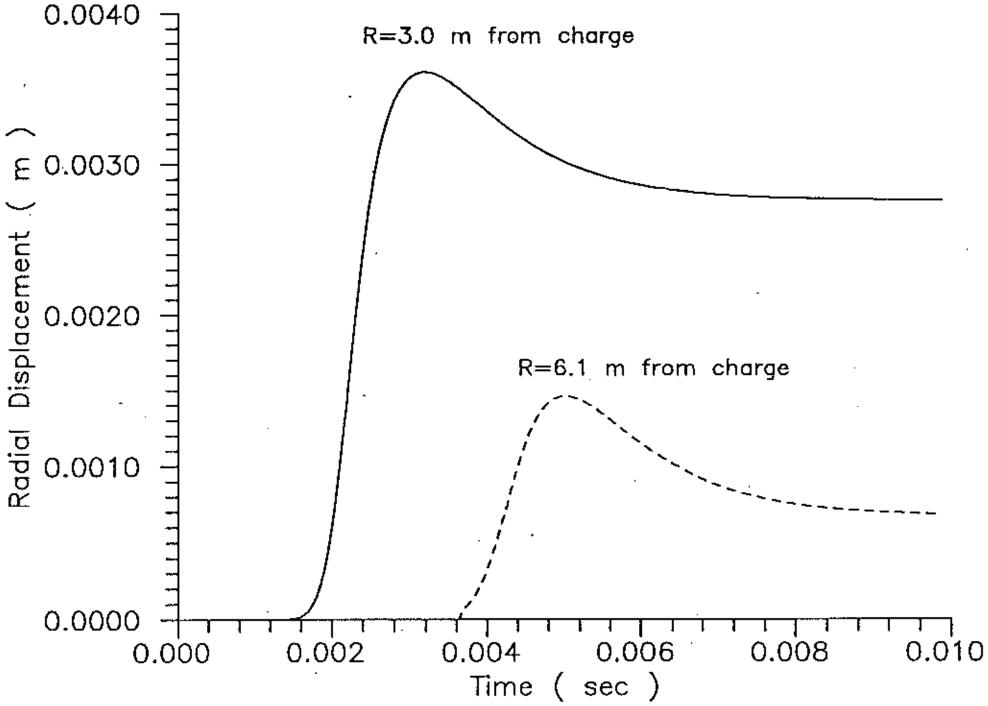

Figure 3.7 Computed Displacement Response for Saturated Loose Sand (W=1.73 kg)

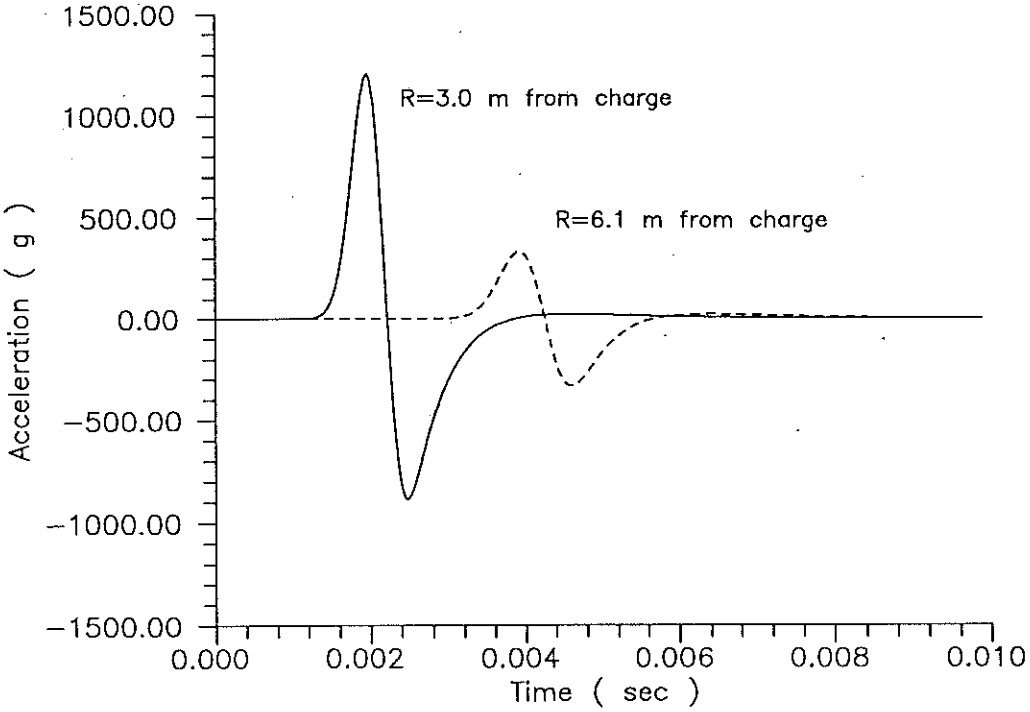

Figure 3.8 Computed Acceleration Response for Saturated Loose Sand (W=1.73 kg)

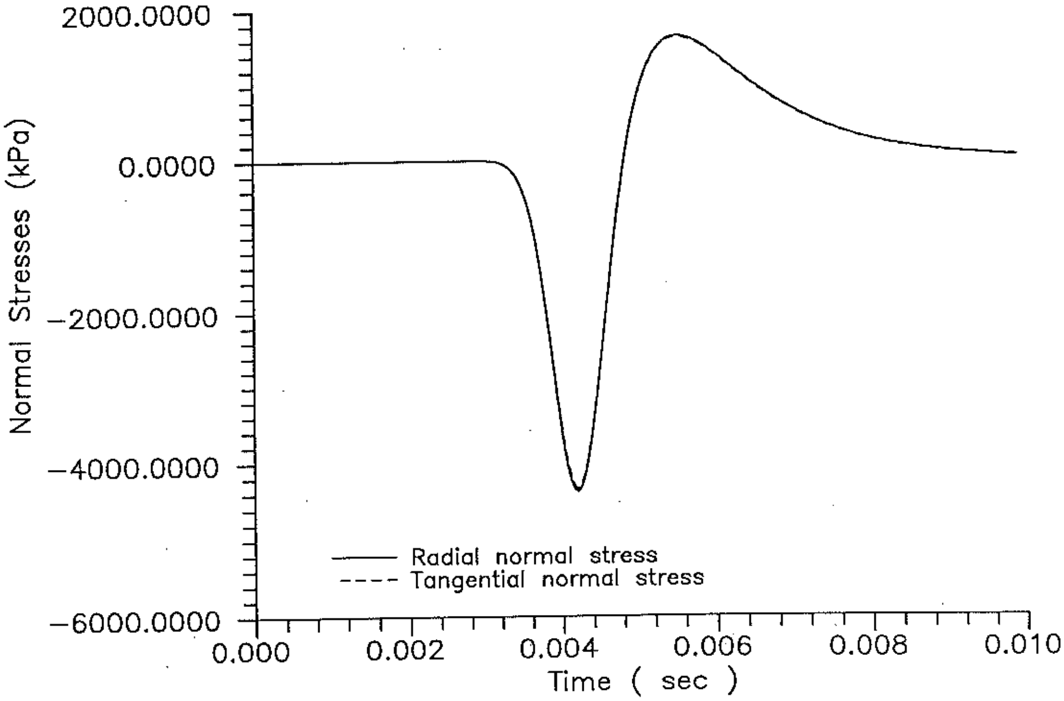

Figure 3.9 Computed Normal Stress Response at r = 6.1 m for Saturated Loose Sand (W=1.73 kg)

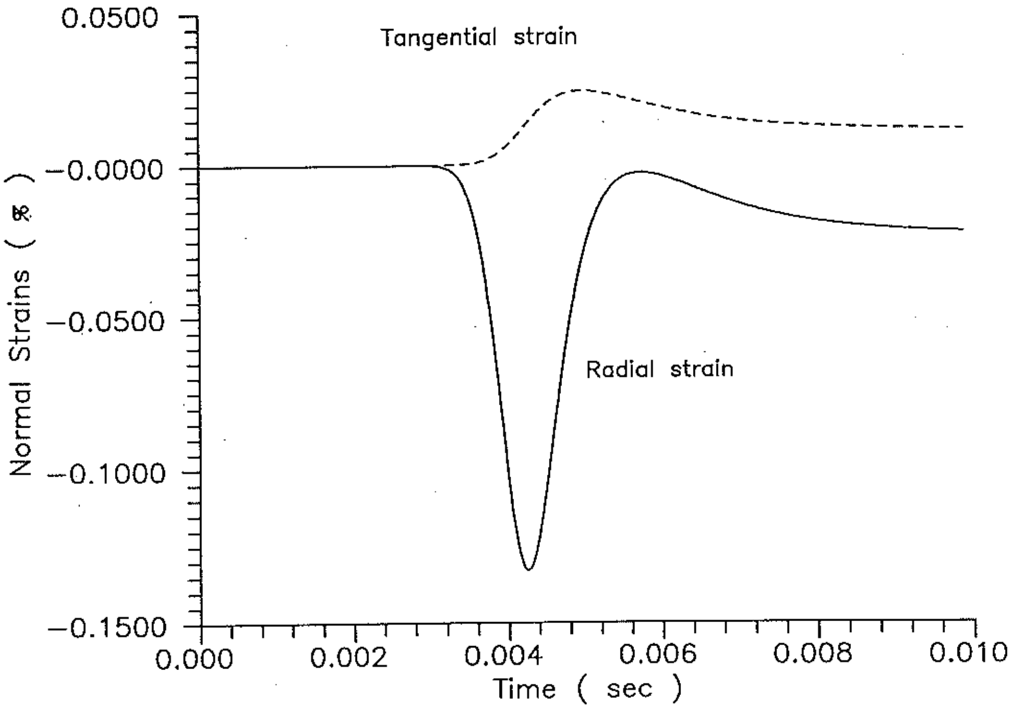

Figure 3.10 Computed Normal Strain Response at r = 6.1 m for Saturated Loose Sand (W=1.73 kg)

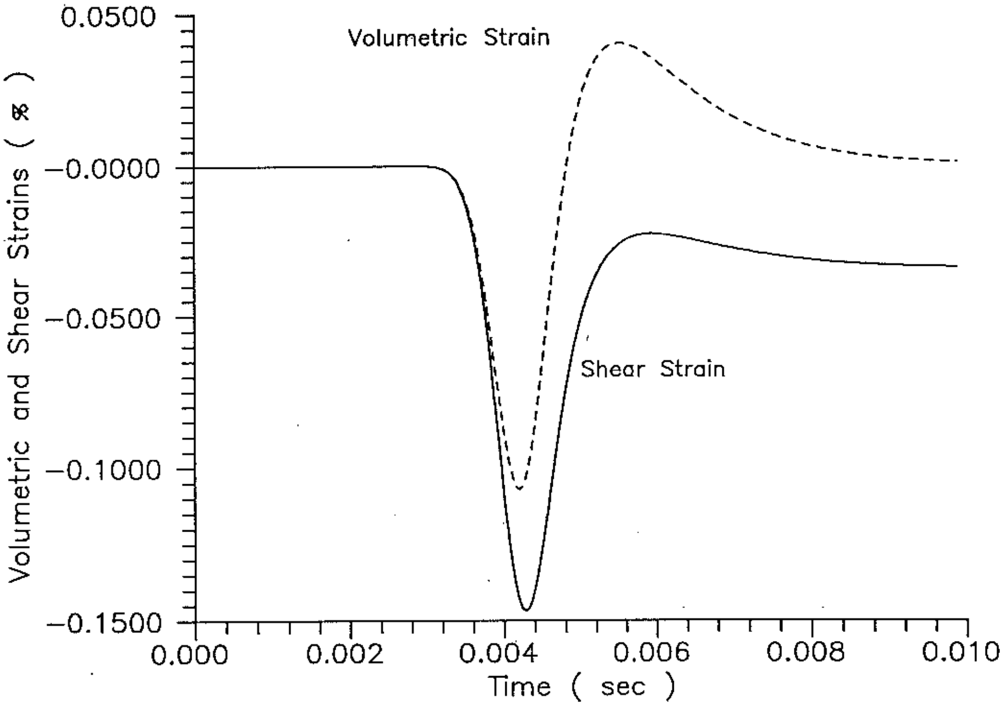

Figure 3.11 Computed Volumetric and Shear Strains at r = 6.1 m for Saturated Loose Sand (W=1.73kg)

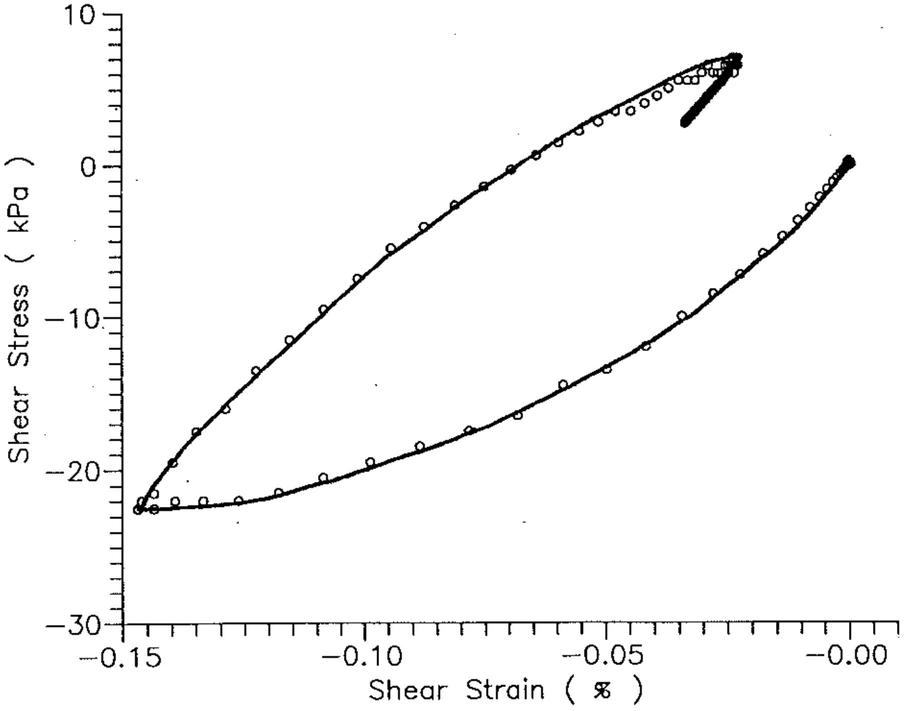

Figure 3.12 Computed Shear Stress-Strain Loop at r = 6.1 m for Saturated Loose Sand (W=1.73 kg)

Peak Dynamic Response Versus Scaled Distance

Analyses are performed to study the relationships between peak dynamic water pressures, accelerations, particle velocities, shear strains, volumetric strains and the scaled distance $R/W^{0.333}$ for charges ranging from 0.1 kg to 8.0 kg. Results of analyses are presented in Figure 3.13 to 3.17. The peak dynamic water pressures and accelerations measured by Hryciw (1986) and listed in Table 3.2 are also shown in Figures 3.13 and 3.15. Although Hryciw's test data were obtained corresponding to charge weights of W = 1.73 kg, these data are used to show relationships between the peak dynamic response over a range of scaled distances for comparison with computed results. The computed peak dynamic water pressures are in fairly good agreement with the measured ones at the same scaled distance. However the computed peak accelerations are less than measured accelerations at the same scaled distance.

A comparison of computed and measured peak particle velocities versus the scaled distance is shown in Figure 3.14. It is noted that the peak particle velocities measured at the soil surface are lower than the computed peak particle velocities at the same distance within the saturated loose sand. This discrepancy is attributed to two major factors; the existence of an unsaturated upper layer of soil and free surface effects due to wave reflections at the ground surface. It is noted that the ground water table of the test site at the time of blasting was at some depth below the ground surface. Therefore, the shock wave passed through an unsaturated soil zone before it reached the ground surface. This unsaturated zone may have significantly reduced the magnitude of the shock wave since an unsaturated zone has a much lower compressive wave velocity relative to the saturated case.

Typically at $r = 4.0$ m away from a charge of 1.0 kg, the numerical model predicts a peak dynamic water pressure of 6000 kPa, a peak acceleration of 600 g and a peak particle velocity of 2.5 m/sec. The corresponding shear strain and volumetric strain at $r = 4.0$ m are in the order of 0.2% and 0.15%, respectively. For the same charge, the level of shear strain approaches 1% at $r = 2.0$ m.

The coefficients of viscosity used in this analysis are listed in Table 3.4. Values of η from 22.0 kPa.s to 100 kPa.s were used, corresponding to charge weights from 0.1 kg to 8.0 kg, respectively.

Table 3.4 Coefficients of viscosity η corresponding to charge weight W used in the modelling of saturated loose sand (V_P = 1540 m/s)

W (kg)	0.1	0.5	1.0	2.0	4.0	8.0
η (kPa.s)	22.0	40.0	50.0	63.0	80.0	100.0

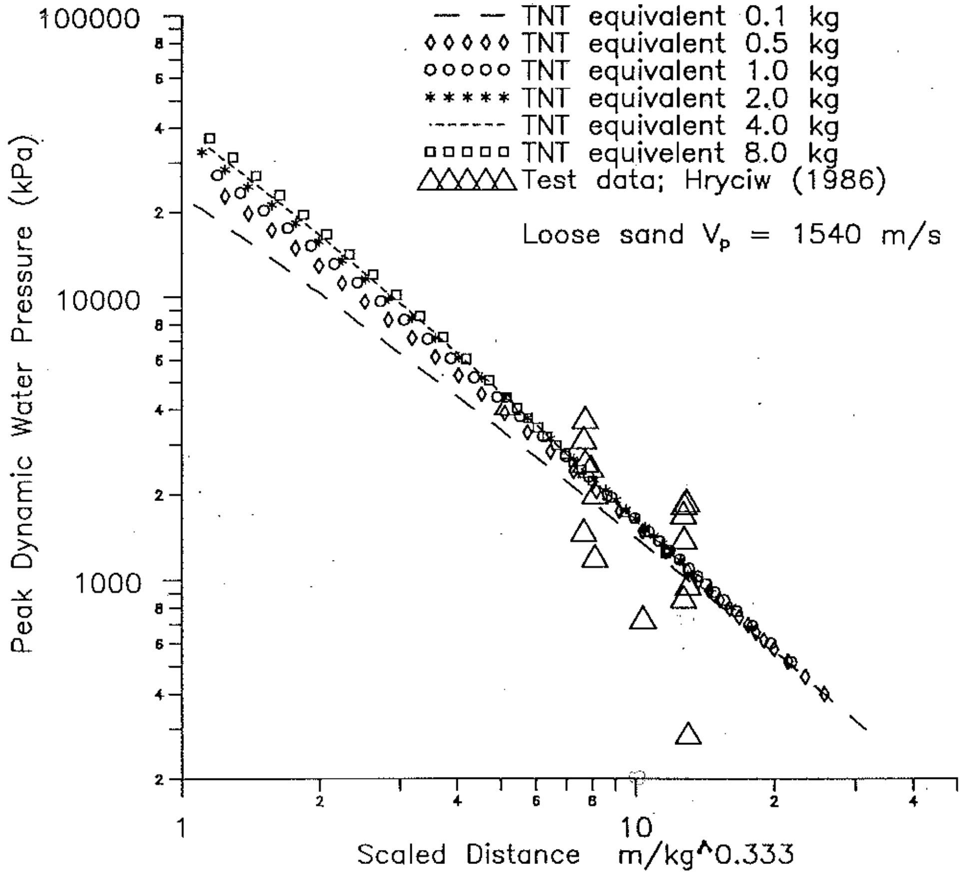

Figure 3.13 Computed Peak Water Pressures vs. Scaled Distance R/W$^{0.333}$ in Saturated Loose Sand

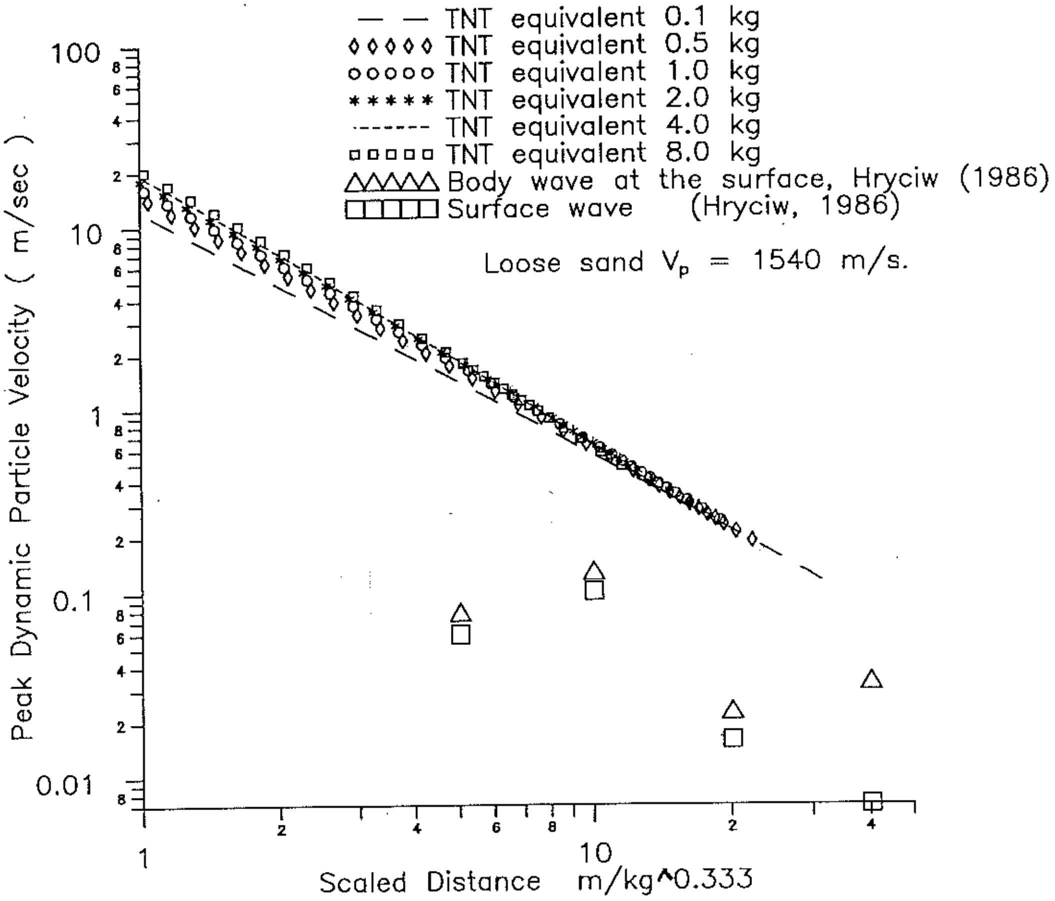

Figure 3.14 Computed Peak Particle Velocities vs. Scaled Distance $R/W^{0.333}$ in Saturated Loose Sand

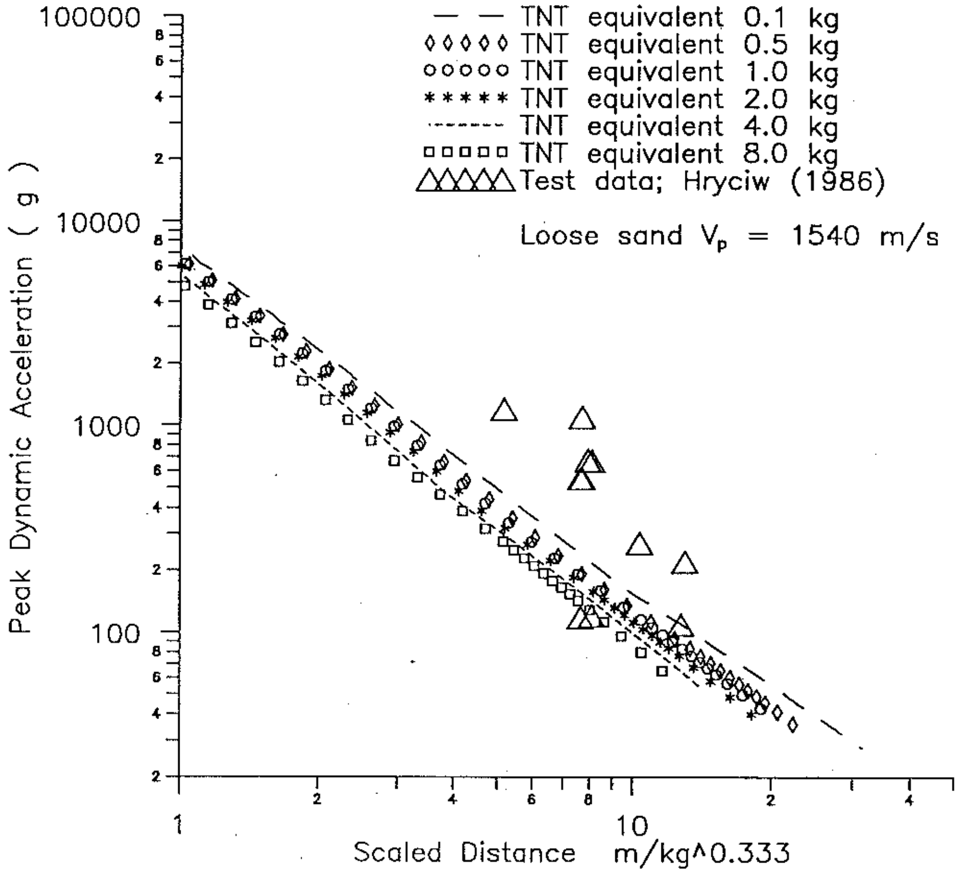

Figure 3.15 Computed Peak Accelerations vs. Scaled Distance $R/W^{0.333}$ in Saturated Loose Sand

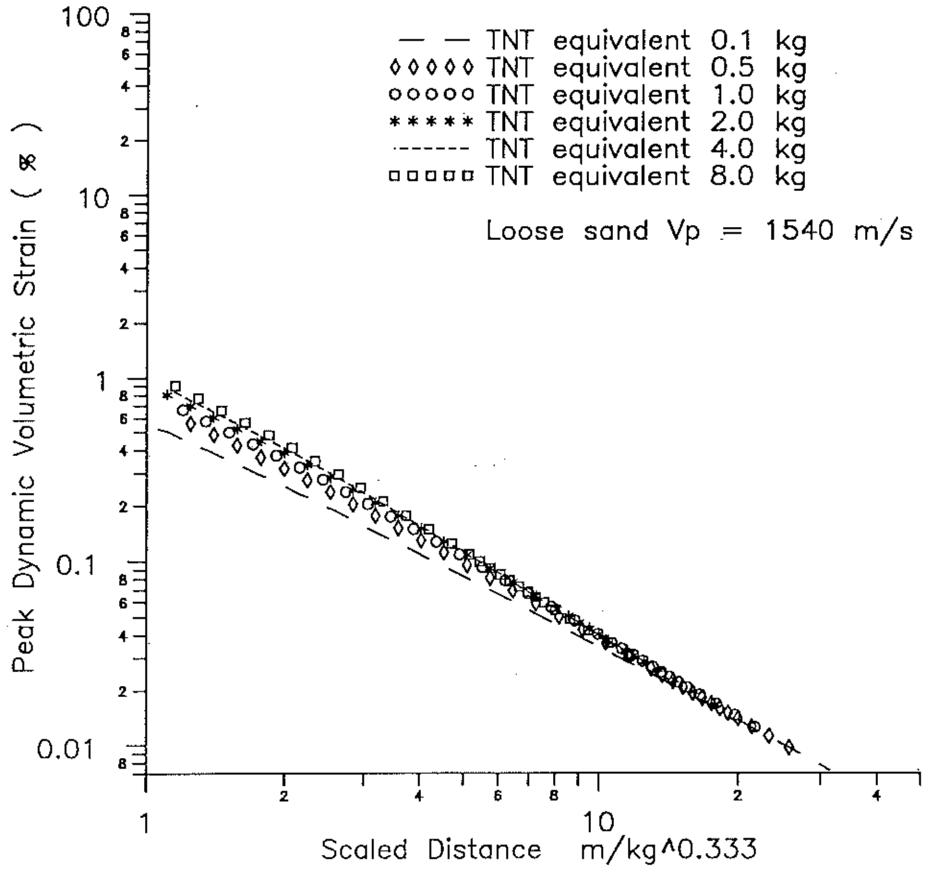

Figure 3.16 Computed Peak Dynamic Volumetric Strains vs. Scaled Distance $R/W^{0.333}$ in Saturated Loose Sand

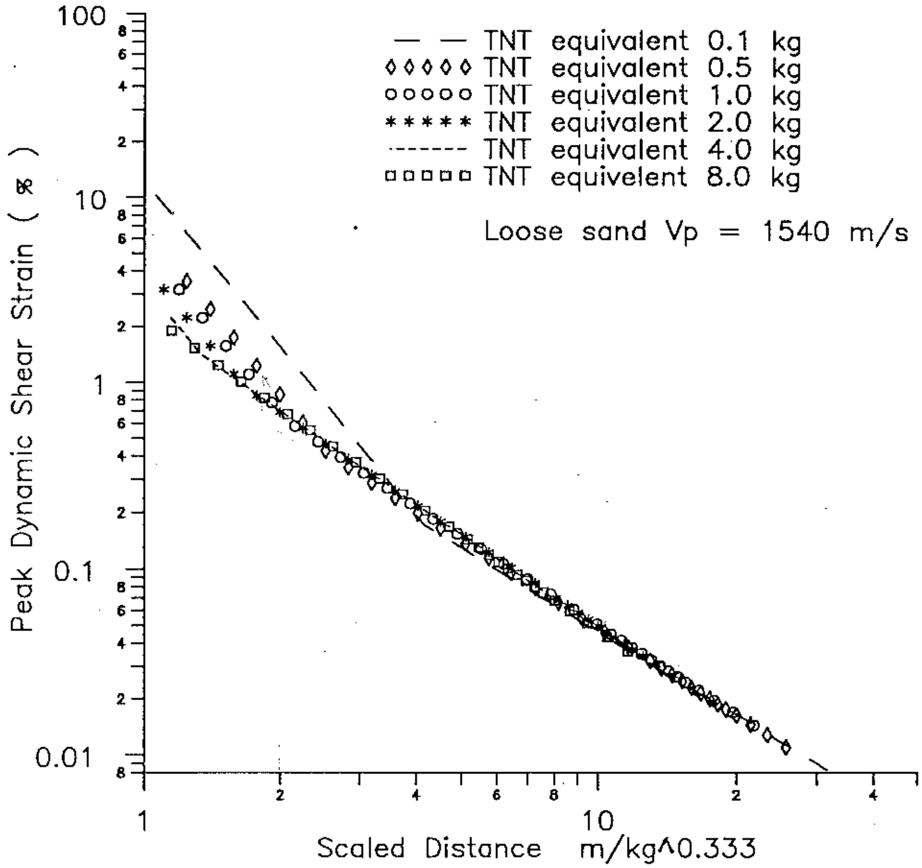

Figure 3.17 Computed Peak Dynamic Shear Strain vs. Scaled Distance R/W$^{0.333}$ in Saturated Loose Sand

3.3.4 Nonlinear Dynamic Response of a Dense Sand Deposit to Blast Loads

Test Results

Jacobs (1988) and Charlie et al. (1992) reported test results showing measured peak particle velocities and dynamic water pressures at various distances from buried charges placed in dense sand. In the tests, single charges were fired having charge weights varying from 0.045 kg to 9.10 kg (TNT equivalent from 0.068 kg to 8.14 kg). Explosives utilized in the tests were Primacord and Tovex 800. Primacord has an energy rating of 1500 calories per gram (50% greater than TNT) and a detonation velocity of 6700 m/sec. Tovex 800 has an energy rating of 894 calories per gram (89% of TNT) and a detonation velocity of 4800 m/sec. Charges were located 3.0 m below the ground surface. Dynamic water pressures were also measured at 3.0 m below the ground surface, but the particle velocities were measured at 1.0 m below the ground surface or 0.1 m below the ground water table. The test results are summarized in Table 3.5.

Table 3.5 Peak Dynamic Water Pressures and Peak Particle Velocities Measured in a Dense Sand (after Jacobs, 1988)

Actual Charge Weight (kg)	TNT equivalent (kg)	Hypocentral Distance (m)	Peak Velocities (m/sec)	Peak Pore water Pressures (kPa)
Primacord 0.0453	0.068	6.10	0.053	121.35
Tovex 0.091	0.0814	6.10	0.057	122.73
Tovex 0.091	0.0814	12.2	0.017	NR
Tovex 0.453	0.405	6.10	0.152	635.03
Tovex 0.453	0.405	12.20	0.033	17.240
Tovex 2.264	2.024	6.10	0.188	875.66
Tovex 2.264	2.024	12.20	0.036	94.46
Tovex 9.103	8.138	30.5	0.037	NA
Tovex 9.103	8.138	13.5	0.306	NA
Tovex 9.103	8.138	15.5	NA	652.26
Tovex 9.103	8.138	19.2	NA	513.68

NR --- no response recorded; NA -- data not available

Charges were placed within a saturated, dense alluvial sand deposit. The measured shear wave velocities varied from 190 m/sec at a depth of 0.5 m to 270 m/sec at a depth of 3.65 m. The compressive wave velocity deduced from arrival times of shock waves was in the range of 1656 m/sec to 1700 m/sec. Cone penetration tests showed that the relative density of the sand ranged from 70% to 90%.

Computed Dynamic Response

This field test was analyzed using the numerical model discussed above. The analysis used a shear wave velocity V_s = 250 m/sec, a compressive wave velocity V_p = 1700 m/sec, a shear strength τ_{max} = 70 kPa, and a unit weight γ = 17.0 kN/m^3. The coefficients of viscosity used in the analyses ranged from 75 kPa.s for small charges to 320 kPa.s for large charges. Table 3.6 gives the coefficients of viscosity used in the analysis for charges having TNT equivalents ranging from 0.1 kg to 8.0 kg.

Table 3.6 Coefficients of viscosity η corresponding to charge weight W used in the modelling of saturated dense sand (V_P = 1700 m/s)

W (kg)	0.1	0.5	1.0	2.0	4.0	8.0
η (kPa.s)	75.0	127.0	160.0	200.0	255.0	320.0

The computed peak dynamic water pressures and peak particle velocities are plotted against the scaled distance $R/W^{0.333}$ (R=distance in m, W = TNT equivalent charge weight in kg) in Figures 3.18 and 3.19, respectively. The measured responses presented by Jacobs are also presented in these figures for comparison. It can be seen that the numerical model predicts dynamic responses that are in good agreement with the measured field responses.

Computed peak accelerations are plotted against scaled distance in Figure 3.20. Dynamic volumetric strains and shear strains are also computed from the analysis and are shown in Figures 3.21 and 3.22, respectively.

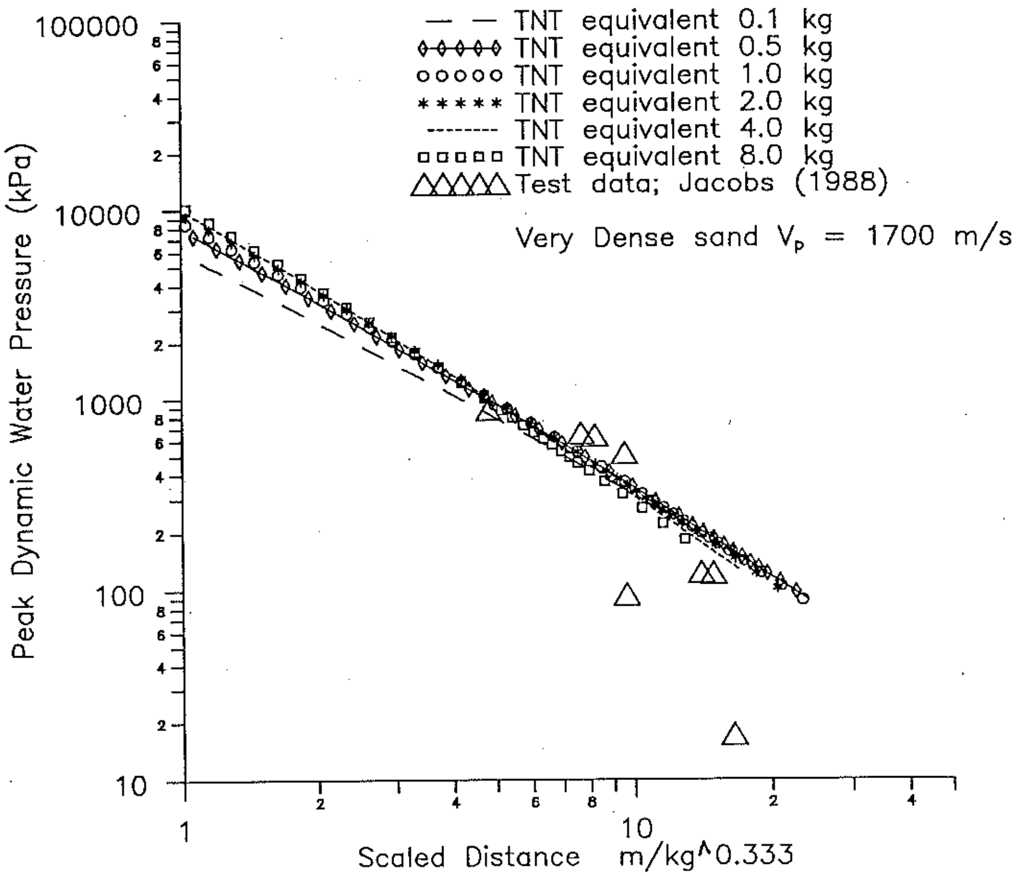

Figure 3.18 Computed Peak Dynamic Water Pressures vs. Scaled Distance R/W$^{0.333}$ in Saturated Dense Sand

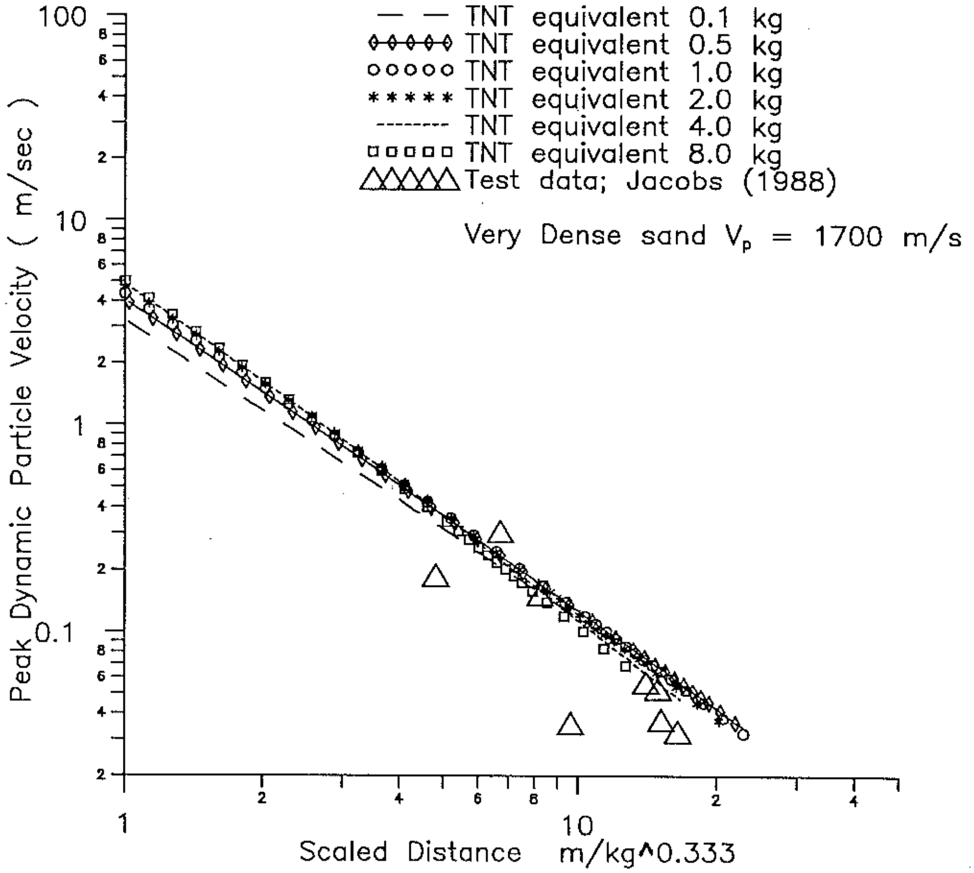

Figure 3.19 Computed Peak Particle Velocities vs. Scaled Distance $R/W^{0.333}$ in Saturated Dense Sand

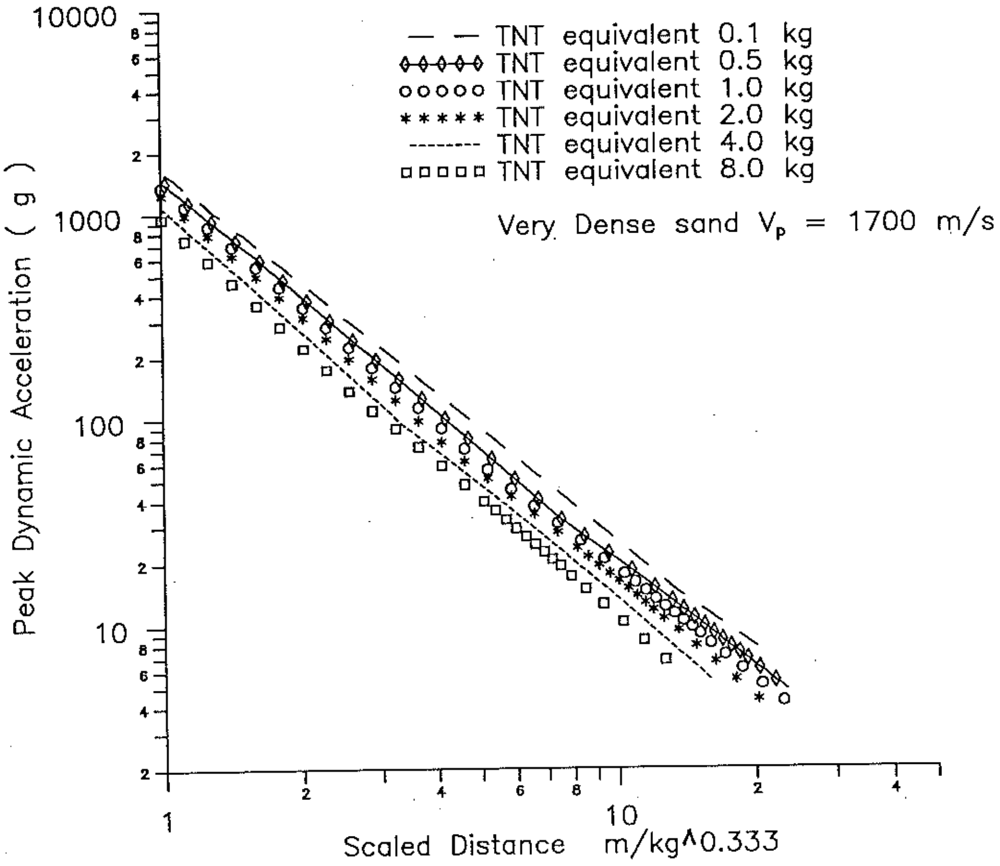

Figure 3.20 Computed Peak Accelerations vs. Scaled Distance $R/W^{0.333}$ in Saturated Dense Sand

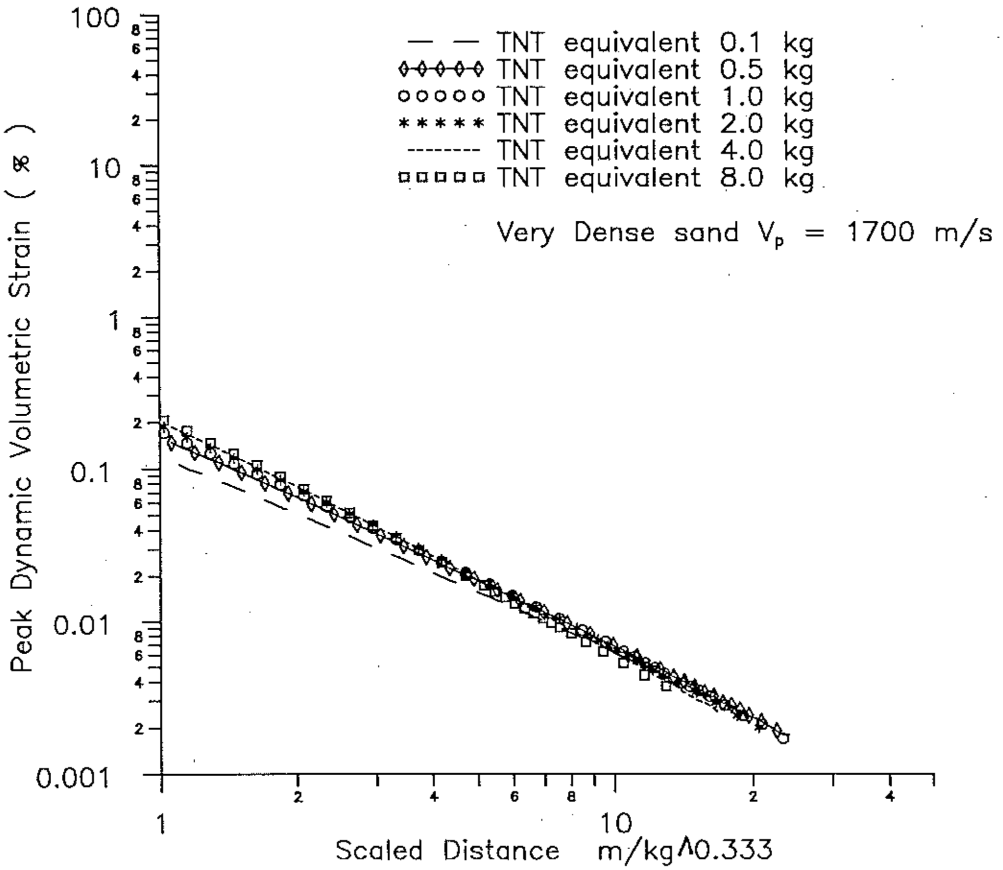

Figure 3.21 Computed Peak Dynamic Volumetric Strains vs. Scaled Distance $R/W^{0.333}$ in Saturated Dense Sand

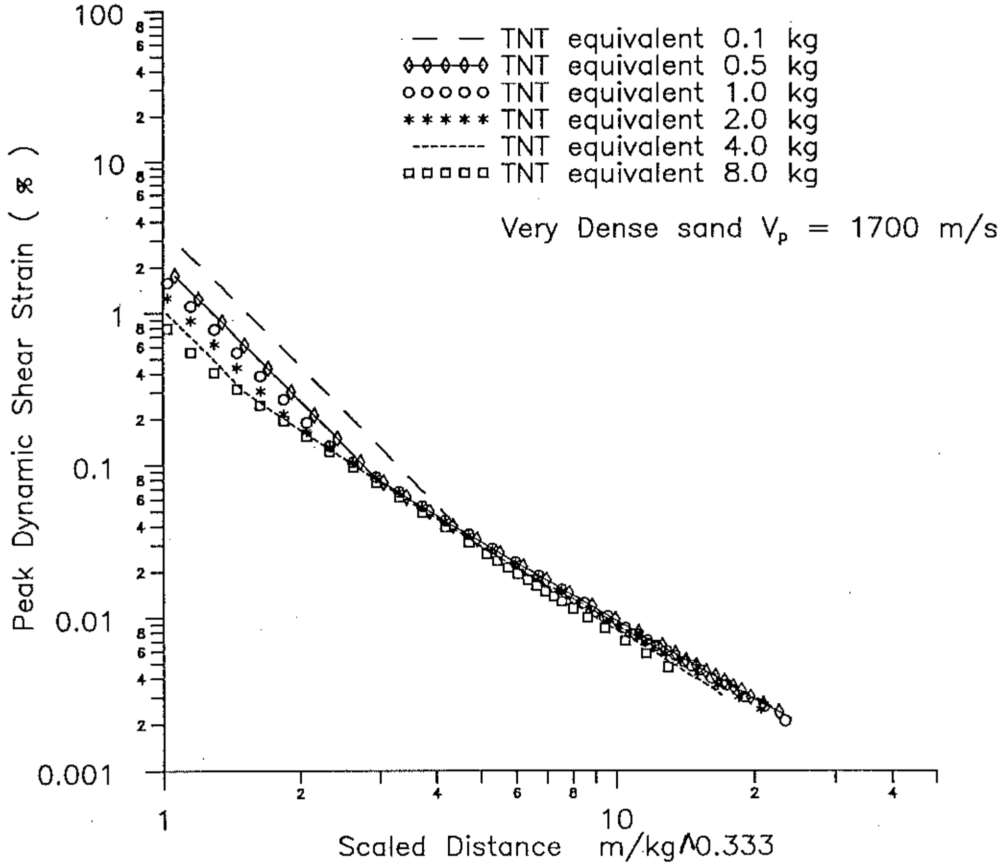

Figure 3.22 Computed Peak Dynamic Shear Strain vs. Scaled Distance R/W$^{0.333}$ in Saturated Dense Sand

3.4. Relationship between Viscosity, Compressive Wave Velocity and Charge Weight

The soil-water viscosity of saturated granular soils has been found to increase with charge weight and compressive wave velocity. Table 3.7 and Figure 3.23 summarize the coefficients of viscosity used for blast modelling in water, saturated loose sand and saturated dense sand. This relationship is established in such a way that the peak dynamic response computed from the numerical model matches the measured field response.

Table 3.7 Coefficients of viscosity η corresponding to charge weight W used in the modelling of water, loose sands and saturated dense sands

W (kg)	0.1	0.5	1.0	2.0	4.0	8.0
η(kPa.s) for water	7.0	13.0	17.0	22.0	28.0	35.0
η(kPa.s) for loose sands	22.0	40.0	50.0	63.0	80.0	100.0
η(kPa.s) for dense sands	75.0	127.0	160.0	200.0	255.0	320.0

The following equation is proposed to describe the relationship between the coefficient of viscosity η and the charge weight W,

$$\eta = K_{\eta} \cdot W^{0.333} \tag{58}$$

where η = viscosity coefficient in kPa.s
W = TNT equivalent charge weight in kg
K_{η} = viscosity number corresponding to the coefficient of viscosity at W=1.0 kg

The numerical studies carried out to date suggest that the viscosity number for a material is reasonably constant. For water, loose sand and dense sand, the viscosity number K_{η} is found to be 17, 50, 160, respectively.

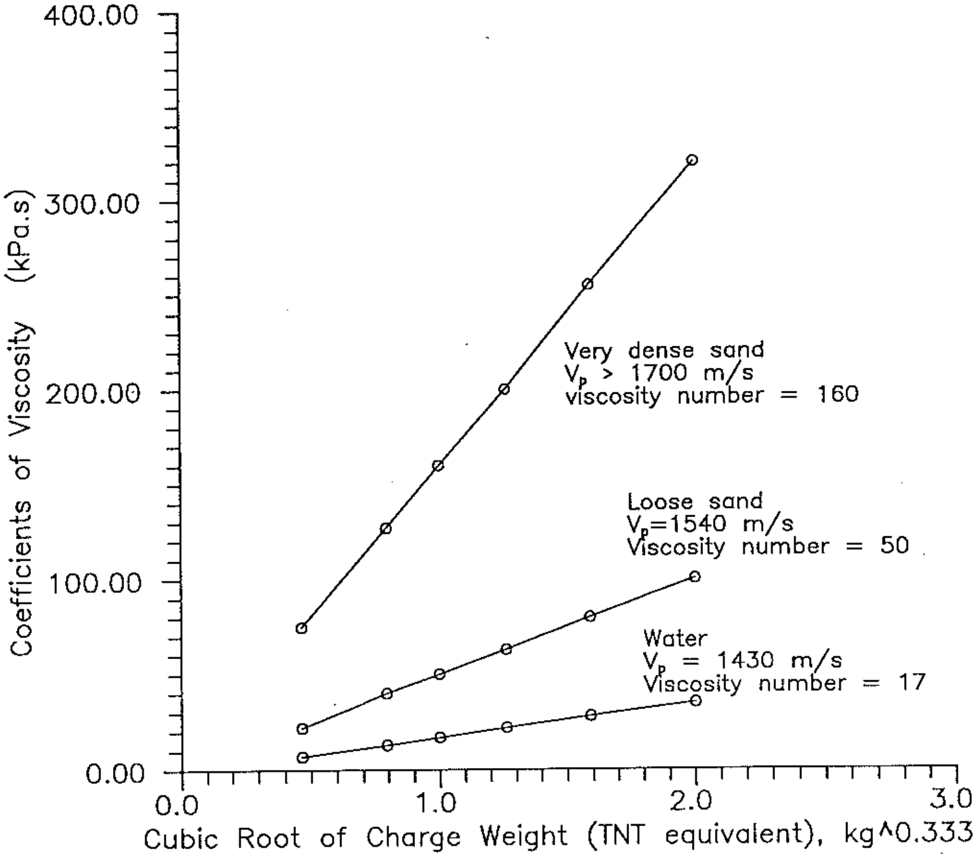

Figure 3.23 Tentative Relationships between Coefficients of Viscosity and Charge Weight for Water, Saturated Loose and Dense Sands

3.5 Summary and Discussion

The results presented in this chapter strongly support the argument that the peak dynamic soil response, such as peak dynamic water pressure and particle velocity, depends strongly on the relative density of saturated sand. Dynamic response in loose sand is greater than in dense sand. The computed peak dynamic water pressures and particle velocities for water, loose sand and dense sand are presented against the scaled distance $R/W^{0.333}$ in Figure 3.24 and Figure 3.25, respectively.

The dynamic finite elements studies carried out require fundamental soil properties such as soil density, shear wave velocity V_s, compressive wave velocity V_p and the shear strength of the soil. Parametric studies have revealed that the shear strength and the shear wave velocity have a relatively small impact on the computed dynamic response while the compressive wave velocity has a greater influence.

A key parameter required in the numerical analysis is the coefficient of viscosity of the soil-water mixture which depends on degree of saturation, relative density and charge weight. During blasting, the viscous behaviour of soil appears to be quite different from what it is under conditions of earthquake loading. Preliminary studies show that the coefficients of viscosity are in the range of 20 kPa.s to 300 kPa.s for saturated granular soils. This parameter can not be directly measured using commonly available testing techniques.

Test blasting is usually required to provide field response data to permit calibration of the viscosity parameter for a specific site condition. During a test blast, it is suggested that peak dynamic particle velocities and peak dynamic pore water pressures be measured at several locations within the soil mass. The coefficient of viscosity would then be determined by matching the computed peak dynamic responses with the measured responses.

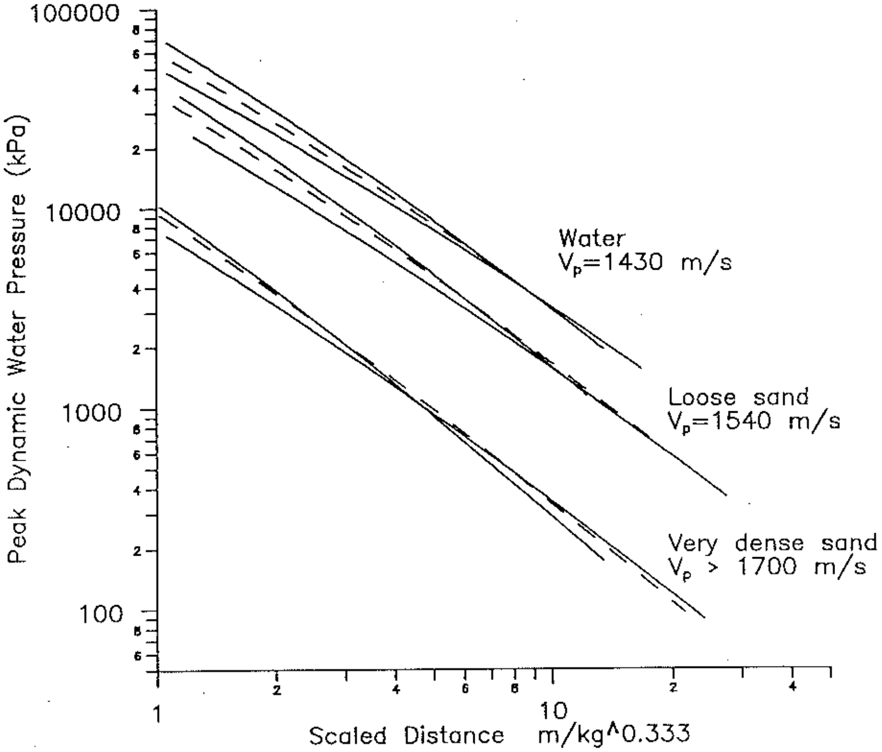

Figure 3.24 Computed Ranges of Peak Dynamic Water Pressures within Water, Saturated Loose and Dense Sands

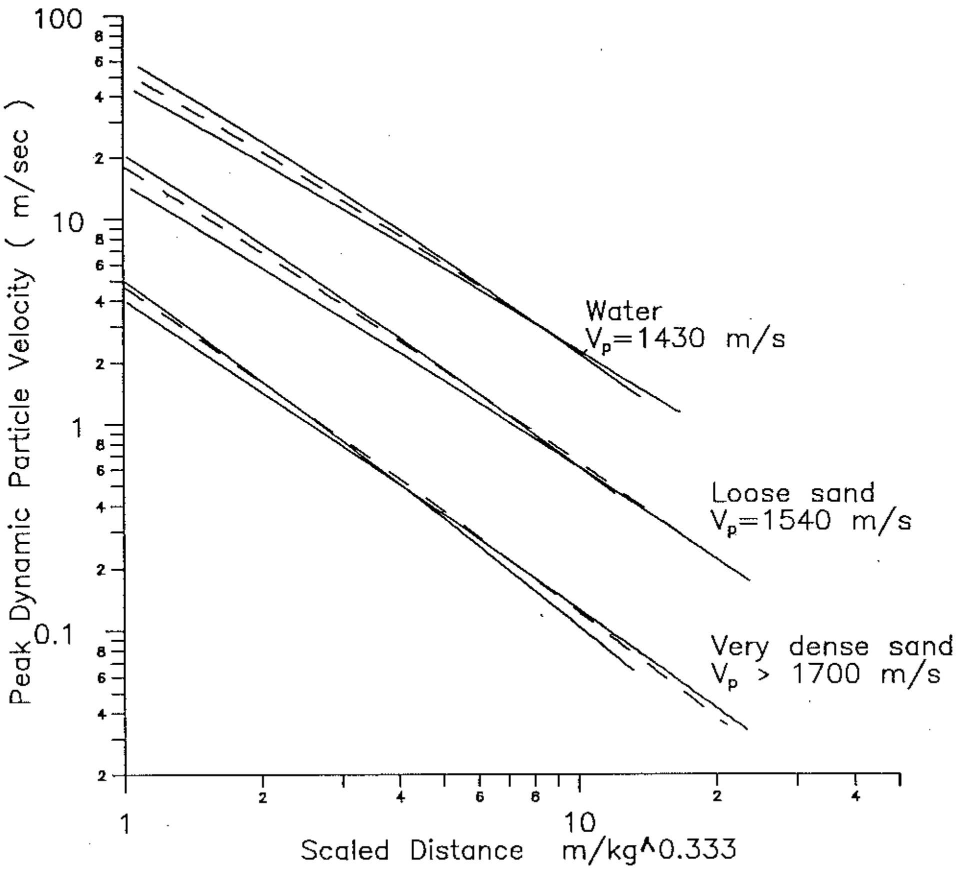

Figure 3.25 Computed Ranges of Peak Particle Velocities within Water, Saturated Loose and Dense Sands

4.0 CONCLUSIONS

In this report, a 3D spherically symmetric finite element method is presented for linear and nonlinear response analysis of soil media subjected to blast loads. The saturated soil material is modelled as a bonded, single phase medium. A nonlinear shear stress-shear strain relationship is used to simulate the shear resistance of the material to shear strain, and a viscosity formulation is presented for modelling the dependence of the shear resistance of the material to the time rate of shear strain. Under linear elastic conditions, the proposed numerical method gives exactly the same solutions as the closed-form solutions presented by Sharpe (1942).

Under nonlinear conditions, studies presented in this report lead to the following findings:

1. The viscosity of the saturated soil has the greatest effect on dynamic response of the material. The increase of viscosity significantly reduces the level of computed dynamic response.

2. Numerical studies carried out to date show that the coefficient of viscosity η increases with the relative density of a granular soil and the charge weight W. It is proposed that the coefficient of viscosity be represented by an equation of the form:

$$\eta = K_{\eta} \cdot (W)^{0.333}$$

where η = viscosity coefficient in kPa.s
W = TNT equivalent charge weight in kg
K_{η} = viscosity number corresponding to the coefficient of viscosity at W=1.0 kg

The viscosity numbers K_{η} for water, saturated loose and dense sands have been determined to be 17, 50, and 160, respectively. These numbers are tentative because of a limited data base and should be re-calibrated on a site specific basis before they are used in practice.

3. Generally, the dynamic response is higher in a loose sand than in a dense sand. Tentative relationships between peak dynamic water pressures, peak particle velocities and the scaled distance $R/W^{0.333}$ for water, saturated loose and dense sands are presented in Figures 3.24 and 3.25, respectively.

4. The shear strains induced by blast loads are very significant, especially in close proximity to a charge. When a charge of 1.0 kg is placed in a saturated loose sand, the induced peak shear strain is about 0.2% at $r = 4.0$ m away from the charge, and may exceed 1% within a radius of $r = 2.0$ m. The significant shear straining caused by blasting is believed responsible for a major portion of the plastic volumetric strain and consequent soil settlement.

5. The peak dynamic volumetric strain is generally less than the peak shear strain.

6. The peak particle velocities measured at the ground surface are believed to be significantly less than those within the saturated soil. The reduction in particle velocity at the ground surface is attributed to two major factors; the existence of an unsaturated zone near the soil surface and wave reflections at the ground surface. A more accurate solution to the dynamic response at the soil surface could likely be obtained using an axial symmetric model instead of a spherically symmetric model presented in this report.

Additional research is currently underway to compute the plastic volumetric strains and residual pore water pressures induced by blasting and will be presented in the next report to NSERC. It is anticipated that the plastic volumetric strains will be related to dynamic shear strains. Residual pore water pressures in saturated sands may then be computed from the computed plastic volumetric strains using the rebound characteristics of the material. Ground surface settlements may also be estimated from the plastic volumetric strains.

Where multiple charges are detonated, the effects of the blast sequence on plastic volume charge, shear strain and pore water pressure will be obtained using the method of supposition. This topic will be presented in the next report to NSERC.

REFERENCE:

1. Barendsen, D.A., and Kok, L. (1983)," Prevention and Repair of Flow-Slides by Explosive Densification," Proc. of 8th European Conf. on Soil Mechanics and Foundations Engineering, Helsinki, pp205-208
2. Charlie, W.A., Jacobs, P.J. and Doehring, D.O. (1992), " Blast - Induced Liquefaction of an Alluvial Sand Deposit," Geotechnical Testing Journal, GTJODJ, Vol. 15, No. 1, March pp14-23
3. Clough, R. W. and Penzien, J., (1975). " Dynamics of Structures," McGraw - Hill Book Company.
4. Cole, R. H. (1948) " Underwater Explosions," Dover Publications Inc., New York
5. Cook, R. D., Malkus, D. S., and Plesha M. E. (1989), " Concepts and Applications of Finite Element Analysis,' 3rd Edition, John Wiley & Sons
6. "Explosive Issue," Ground Engineering, July/August, 1995.
7. Finn, W. D. Liam , Lee, K.W., and Martin, G. R. (1977), " An Effective Stress Model for Liquefaction," Jour. of Geotechnical Engineering Division, ASCE, June, pp 517-533
8. Finn, W. D. Liam, Yogendrakumar, M., Yoshida, N., and Yoshida, H., (1986), " TARA-3: A Program for Nonlinear Static and Dynamic Effective Stress Analysis," Soil Dynamics Group, Dept. of Civil Engineering, Univ. of British Columbia, Vancouver, B.C., Canada
9. Gohl, W.B., Howie, J.A., Hawson, H.H., and Diggle, D. (1994) Field Experience With Blast Densification in an Urban Setting," 5th US Earthquake Conference, Chicago, Illinois, July, pp 221-230.
10. Jacobs, P. J. (1988) "Blast-Induced Liquefaction of an Alluvial Sand Deposit," M.S. thesis, Dept. of Civil Engineering, Colorado State University, Fort Collins, CO, US
11 Hall, C.E. (1962)," Compacting a Dam Foundation by Blasting," Jour. of Soil Mechanics and Foundation Division, ASCE, Vol.88, SM3, pp35-51
12. Hachey, J.E. (1992) Golder Associates. Personal communication re: Washington Department of Transportation South Coldwater Creek bridge abutment densification.
13. Hryciw, R.D., (1986), "A Study of the Physical and Chemical Aspects of Blast Densification of Sand," Ph.D. thesis, Northwestern University, U.S.A.
14. Ishihara, K. (1967), " Propagation of Compressional Waves in a Saturated Soil," Proc. of International Symposium on Wave Propagation and Dynamic Properties of Earth Materials, Albuquerque, New Mexico, U.S., pages 451 - 467

15. Ivanov, P.L. (1967), " Compaction of Noncohesive Soils by Explosions," (translated from Russian), National Information Service Report No. TT 70-57221, U.S. Dept. of Commerce, Springfield, VA, 211 pages

16. Klohn, E.J., Garga, V.K., and Shukin, W. (1981), "Densification of Loose Sand Deposits by Blasting," Proc. of 10th International Conf. on Soil Mechanics and Foundation Engineering, Vol.3, pp.725-730

17. Lee, K. W. (1975), " Mechanical Model for the Analysis of Liquefaction of Horizontal Soil Deposits," Ph.D. thesis, Dept. of Civil Engineering, Univ. of British Columbia, B.C., Canada.

18. Lyman, A.K.B. (1942), " Compaction of Cohesionless Foundation Soils by Explosives," Transactions, ASCE (107), pp1330 - 1348

19. Rogers, B.T., Graham, C.A., and Jefferies, M.G. (1990)," Compaction of Hydraulic Fill Sand in Molikpaq Core," Proc. of 43rd Canadian Geotechnical Conf., Canadian Geotechnical Society

20. Sharpe, J. A. (1942), "The production of Elastic Waves by Explosion Pressures, I and II:" Geophysics, 7, 144-154, 311-321

21. Sharpe, G.J. (1967) " Fluid Flow Analysis," American Elserier Publishing Company, Inc., NewYork, U.S.

22. Skempton, A. W., "The Pore Pressure Coefficients A and B," Geotechnique, 4, pp143 - 147

23. Solymar, Z. V. (1984)," Compaction of Alluvial Sands by Deep Blasting," Canadian Geotechnical Journal, Vol. 21, pp305-321

24. Solymar, Z. V. (1984), " Earth Foundation Treatment at Jebba Dam Site," ASEC Jour. of Geotech. Engineering, Vol. 110, No. 10, pp1415-1430.

25. Wilson, E. L., Farhoomand, L., and Bathe, K. J. (1973)," Nonlinear Dynamic Analysis of Complex Structures, " International Journal of Earthquake Engineering and Structural Dynamics, Vol. 1, No. 3, Jan. - March

26. United States Army Corps of Engineers (1972), " Systematic Drilling and Blasting for Surface Excavation, " Engineering Manual, EM 1110-2-3800, Office of the Chief, United States Army Corps of Engineers, Washington, D.C., 119 pages

APPENDIX I: MASS AND STIFFNESS MATRIX FORMULATIONS OF A 3D SPHERICALLY SYMMETRIC ELEMENT

For the finite element shown in Figure 2.2, the element mass matrix is given by

$$[M_{ij}] = 4\pi\rho\int_{0}^{L} N_i\, N_j\, (R_0+\xi)^2\, d\xi$$

where R_0 = radial coordinate at node 1

L = radial distance of the element

ρ = mass density of the elastic medium

$$[M] = \begin{bmatrix} M_{11} & M_{12} & M_{13} \\ M_{21} & M_{22} & M_{23} \\ M_{31} & M_{32} & M_{33} \end{bmatrix}$$

where $M_{11} = 16\pi\rho(R_0^2\, L/30.0 + R_0\, L^2/120.0 + L^3/840.0)$

$M_{12} = 2\pi\rho(2R_0^2\, L/15.0 - 2L^3/105.0)$

$M_{13} = -2\pi\rho(R_0^2\, L/15.0 + R_0\, L^2/15.0 + L^3/42.0)$

$M_{22} = 64\pi\rho(R_0^2\, L/30.0 + R_0\, L^2/30.0 + L^3/105.0)$

$M_{23} = 8\pi\rho(R_0^2\, L/30.0 + R_0\, L^2/15.0 + L^3/35.0)$

$M_{33} = 16\pi\rho(R_0^2\, L/30.0 + 7R_0\, L^2/120.0 + 11L^3/420.0)$

$M_{ji} = M_{ij}$

The element stiffness matrix is given by

$$[K] = \int_{\Omega} \left(\frac{\partial N_i}{\partial R}\ \frac{N_i}{R}\ \frac{N_j}{R}\right) \begin{bmatrix} \lambda+2G & \lambda & \lambda \\ \lambda & \lambda+2G & \lambda \\ \lambda & \lambda & \lambda+2G \end{bmatrix} \begin{pmatrix} \dfrac{\partial N_i}{\partial R} \\ \dfrac{N_i}{R} \\ \dfrac{N_j}{R} \end{pmatrix} (4\pi R^2)dR$$

where $R = R_0 + \xi$

G = shear modulus

λ = Lame's constant, $\lambda = B - 2/3 * G$

B = bulk modulus

i.e.

$$[K_{ij}] = 4\pi \int_0^L [(R_0+\xi)^2(\lambda+2G)\frac{\partial N_i}{\partial \xi}\frac{\partial N_j}{\partial \xi}+2\lambda(R_0+\xi)(N_i\frac{\partial N_j}{\partial \xi}+N_j\frac{\partial N_i}{\partial \xi})+4(\lambda+G)N_iN_j]\ d\xi$$

The element stiffness matrix is given in matrix form as

$$[K] = \begin{bmatrix} K_{11} & K_{12} & K_{13} \\ K_{21} & K_{22} & K_{23} \\ K_{31} & K_{32} & K_{33} \end{bmatrix}$$

where $K_{11} = 4\pi((\lambda+2G)(7/3*R_0^2 /L - R_0 + 7/15*L) + 4R_0 G)$

$K_{12} = -16/15*\pi(\lambda+2G)*(10R_0^2 /L + 5R_0 + L)$

$K_{13} = 4/15*\pi(\lambda+2G)*(5R_0^2/ L + 5R_0 + 2 L)$

$K_{22} = 64\pi(\lambda+2G)*(1/3*R_0^2/L + 1/3*R_0 + 0.2*L)$

$K_{23} = -16/15*\pi(\lambda+2G)(10R_0^2 /L + 15R_0 + 6L)$

$K_{33} = 4\pi((\lambda+2G)*(7/3*R_0^2 /L + 11/3*R_0 + 27/15*L) + 2*\lambda(R_0+L))$

$K_{ji} = K_{ij}$

The damping matrix [C] due to viscosity has the same form as the stiffness matrix [K]. However, in damping matrix [C] the shear modulus G is replaced by the viscosity coefficient η and bulk modulus $B=0$.

APPENDIX II: ANALYTICAL SOLUTIONS BY SHARPE (1942)

The equation governing the dynamic response of the elastic medium around the cavity is given by

$$(\lambda+2G)\left(\frac{\partial^2\phi}{\partial r^2}+\frac{2}{r}\frac{\partial\phi}{\partial r}\right)=\rho\frac{\partial^2\phi}{\partial t^2}$$

where ϕ = displacement potential
t = time
r = radial coordinate

The radial displacement u_r along the radial direction of a charge is determined from the displacement potential ϕ by $u_r = \partial\phi / \partial r$.

Applying boundary condition $p(r,t)_{r=a} = P_0 e^{-\alpha t}$, solutions were found by Sharpe (1942) as

$$\phi=\frac{P_0 a}{\rho[\omega_0^2+(\alpha_0-\alpha)^2]}[e^{-\alpha_0 T}[\cos(\omega_0 T)+\frac{\alpha_0-\alpha}{\omega_0}\sin(\omega_0 T)-e^{-\alpha T}]$$

where $\alpha_0 = V_P(1-2\mu)/(1-\mu)/a$
$\omega_0 = V_P(1-2\mu)^{0.5}/(1-\mu)/a$ a = cavity radias
$T = t - (r-a)/V_P$
μ = Poisson's ratio
V_P = compressive wave velocity

The radial displacement u_r is obtained as

$$u_r=\frac{P_0 a}{r^2\rho[\omega_0^2+(\alpha_0-\alpha)^2]}\{-[e^{-\alpha_0 T}(\cos(\omega_0 T)+\frac{\alpha_0-\alpha}{\omega_0}\sin(\omega_0 T))-e^{-\alpha T}]$$

$$+\frac{r}{V_P}[e^{-\alpha_0 T}(\alpha\cos(\omega_0 T)+\frac{\omega_0^2+\alpha_0^2-\alpha_0\alpha}{\omega_0}\sin(\omega_0 T))-\alpha e^{-\alpha T}]\}$$

Radial velocity $\{\partial u_r/\partial t\}$, acceleration $\{\partial^2 u_r/\partial t^2\}$ and radial strain $\{\varepsilon_r\}$ are obtained according to their relationship with the radial displacement u_r. The formulae for these variables are given as follows:

$$\frac{\partial u_r}{\partial t} = \frac{P_0 a}{r^2\rho[\omega_0^2+(\alpha_0-\alpha)^2]}\{[e^{-\alpha_0 T}(\alpha\cos(\omega_0 T)+\frac{\omega_0^2+\alpha_0^2-\alpha\alpha_0}{\omega_0}\sin(\omega_0 T))-\alpha e^{-\alpha T}]$$

$$+\frac{r}{V_P}[e^{-\alpha_0 T}((\omega_0^2+\alpha_0^2-2\alpha_0\alpha)\cos(\omega_0 T))-\frac{\alpha_0\omega_0^2+\alpha\omega_0^2+\alpha_0^3-\alpha\alpha_0^2}{\omega_0}\sin(\omega_0 T))+\alpha^2 e^{-\alpha T}]\}$$

$$\frac{\partial^2 u_r}{\partial t^2} = \frac{P_0 a}{r^2\rho[\omega_0^2+(\alpha_0-\alpha)^2]}\{e^{-\alpha_0 T}[(\omega_0^2+\alpha_0^2-2\alpha_0\alpha)\cos(\omega_0 T)-\frac{\alpha_0\omega_0^2+\alpha\omega_0^2+\alpha_0^3-\alpha\alpha_0^2}{\omega_0}$$

$$\sin(\omega_0 T)] + \alpha^2 e^{-\alpha T}\}+\frac{P_0 a}{rV_P\rho[\omega_0^2+(\alpha_0-\alpha)^2]}\{e^{-\alpha_0 T}[(-2\alpha_0^3+3\alpha\alpha_0^2-2\alpha_0\omega_0^2-\alpha\omega_0^2)\cos(\omega_0 T)$$

$$+\frac{\alpha_0^4-\omega_0^4+3\alpha\alpha_0\omega_0^2-\alpha\alpha_0^3}{\omega_0}\sin(\omega_0 T)] - \alpha^3 e^{-\alpha T}\}$$

The volumetric strain is determined from the normal strains by

$$\varepsilon_v = \varepsilon_r + 2\varepsilon_\theta$$

i.e.

$$\varepsilon_v = \frac{\partial^2\phi}{\partial r^2} + \frac{2}{r}\frac{\partial\phi}{\partial r} = \frac{1}{V_P^2}\frac{\partial^2\phi}{\partial t^2}$$

Therefore volumetric strain ε_v is determined from the displacement potential ϕ as

$$\varepsilon_v = \frac{P_0 a}{V_P^2 r\rho[\omega_0^2+(\alpha_0-\alpha)^2]}\{-e^{-\alpha_0 T}[(\omega_0^2+\alpha_0^2-2\alpha_0\alpha)\cos(\omega_0 T)) - \frac{\alpha_0\omega_0^2+\alpha\omega_0^2+\alpha_0^3-\alpha\alpha_0^2}{\omega_0}$$

$$\sin(\omega_0 T)] - \alpha^2 e^{-\alpha T}\}$$

Since the tangential normal strain ε_θ can be computed from

$$\varepsilon_\theta = \frac{u_r}{r}$$

the radial normal strain ε_r can be calculated as

$$\varepsilon_r = \varepsilon_v - 2\varepsilon_\theta$$

A FORTRAN program is written for computing solutions by Sharpe (1942). The source code of the program is listed as follow.

```
C
      PROGRAM sharpe
      IMPLICIT REAL*8( A-H, O-Z)
C
C      solutions of displacement, velocity, volume change, etc
c     using SHARPE (1942)'s elastic solution
c      A0 = a; radius of cavity;  R = target radial distance
c      P0, ALPHA  p(t) = P0 * exp(-alpha t)
c      ELASTIC parameters:  RHO; G, B
c      NTOTAL; DTIME:   total number of points; dt=DTIME
c
c
      OPEN(UNIT=5, FILE='INP.DAT')
      OPEN(UNIT=6, FILE='OUT.PRN')
C
      READ (5,*)   A0, P0, ALPHA, R
      WRITE(6,102) A0, P0, ALPHA, R
      READ (5,*)   RHO, G, B, EUR
      WRITE(6,104) RHO, G, B, EUR
      READ (5,*)   NTOTAL, DTIME
      WRITE(6,106) NTOTAL, DTIME
 102   FORMAT(2X,' A0, P0, ALPHA, R', 4G12.4)
 104   FORMAT(2X,' RHO, G, B, EUR, ', 4G12.4)
 106   FORMAT(2X,' NTOTAL, DTIME,  ', I6, 4G12.4)
c
      WRITE(6,*) A0, P0, ALPHA, R, EUR, G, B, DTIME
      CALL SHARPE (NTOTAL, RHO, A0, R, B, G, EUR,P0, ALPHA, DTIME)
       STOP
       END
C
C     *************************************************************
      SUBROUTINE SHARPE(NTOTAL, RHO, A0, R, B, G, EUR,
     +           P0, ALPHA, DTIME)
      IMPLICIT REAL*8(A-H,O-Z)
      DIMENSION DISR(10), VOL(10), EPSR(10), EPST(10), GAMM(10)
      DIMENSION PP(10), VELO(10), ACCE(10), SIGR(10)
```

```
C
      ANU = ( 3.0 * B/G -2.0 ) /(6.0 * B/G + 2.0)
      VP  = SQRT( ( B + 4./3.*G) / RHO )
      ALPH0 = VP/A0 * (1.0 - 2.0 * ANU ) / (1.0 - ANU)
      OMEG0 = VP/A0 * SQRT (1.0 - 2.0 * ANU ) / (1.0 - ANU)
      DALPHA = ALPH0 - ALPHA
      B0 = P0 * A0 / RHO /(OMEG0 * OMEG0 + DALPHA * DALPHA)
      B1 = ( OMEG0 * OMEG0 + ALPH0 * ALPH0 - ALPHA * ALPH0 ) / OMEG0
      B2 = 2.0 * ALPHA * ALPH0 - ALPH0 * ALPH0 - OMEG0 * OMEG0
      B3 = (ALPH0*ALPH0*ALPH0 - ALPHA*ALPH0*ALPH0 + ALPH0*OMEG0*OMEG0
     +       + ALPHA * OMEG0 * OMEG0 ) / OMEG0
      B4 = -2.0*ALPH0*ALPH0*ALPH0 + 3.0*ALPHA*ALPH0*ALPH0 -2.0*ALPH0
     +        *OMEG0*OMEG0 - ALPHA * OMEG0 * OMEG0
      B5 = (ALPH0*ALPH0*ALPH0*ALPH0 - OMEG0*OMEG0*OMEG0*OMEG0 + 3.0
     +      *ALPHA*ALPH0*OMEG0*OMEG0 - ALPHA*ALPH0*ALPH0*ALPH0) / OMEG0
      T0 = ( R-A0) / VP
      WRITE(6,*)' ANU, VP, T0, OMEG0, ALPH0, B0,B1,B2,B3,B4,B5'
      WRITE(6,*) ANU, VP, T0, OMEG0, ALPH0, B0,B1,B2,B3,B4,B5
C
C
      DO 100 K = 1, NTOTAL
C
       T = K * DTIME
       KK = 1
C
       A2 = EXP( -ALPH0 * T)
       A3 = EXP( -ALPHA * T)
       A4 = COS( OMEG0 * T )
       A5 = SIN( OMEG0 * T )
C
       DISR(KK) = - B0 /R / R * (A2 * ( A4 + DALPHA / OMEG0 * A5 )
     +          - A3 ) + B0 / VP / R *( A2 * ( ALPHA * A4 + B1 * A5)
     +          - ALPHA *  A3 )
       EPST(KK) = DISR(KK) / R
       VOL (KK) = B0 /VP/VP/R *(A2 *( B2 * A4 + B3 * A5) -
     +            ALPHA * ALPHA * A3)
       EPSR(KK) = VOL(KK) - 2.0 * EPST(KK)
       SIGR(KK) = ( B + 4./3.*G)* EPSR(KK) + 2.0*(B-2./3.*G) *EPST(KK)
       GAMM(KK) = 0.5 * ( EPSR(KK) - EPST(KK) )
```

```
C
      VELO(KK) = B0 /R/R * ( A2 *(ALPHA * A4 + B1 * A5) - ALPHA * A3)
     +        + B0 /VP/R *( A2 * (-B2*A4-B3*A5) + ALPHA*ALPHA*A3 )
      ACCE(KK) = - VP*VP*VOL(KK)/R + B0/VP/R * ( A2 * (B4*A4+B5*A5)
     +        - ALPHA * ALPHA * ALPHA * A3 )
      PVEL = - VP * EPSR(KK)
      WRITE(6, 102) T, DISR(KK), VELO(KK), ACCE(KK), GAMM(KK)
     +      ,VOL(KK), SIGR(KK), PP(KK), PVEL
 100  CONTINUE
 102  FORMAT( F10.6, 10G12.4)
      RETURN
      END
```